



MICS-Asia III: overview of model intercomparison and evaluation of acid deposition over Asia

Syuichi Itahashi^{1,2}, Baozhu Ge^{3,4,5}, Keiichi Sato⁶, Joshua S. Fu⁷, Xuemei Wang⁸, Kazuyo Yamaji⁹, Tatsuya Nagashima^{10,11}, Jie Li^{3,4,5}, Mizuo Kajino^{2,11}, Hong Liao¹², Meigen Zhang^{3,4,5}, Zhe Wang^{3,13}, Meng Li¹⁴, Junichi Kurokawa⁶, Gregory R. Carmichael¹⁵, and Zifa Wang^{3,4,5}

¹Environmental Science Research Laboratory, Central Research Institute of Electric Power Industry (CRIEPI), Abiko, Chiba 270–1194, Japan

²Meteorological Research Institute (MRI), Tsukuba, Ibaraki 305–0052, Japan

³State Key Laboratory of Atmospheric Boundary Layer Physics and Atmospheric Chemistry (LAPC), Institute of Atmospheric Physics (IAP), Chinese Academy of Sciences (CAS), Beijing 100029, China

⁴Collage of Earth Science, University of Chinese Academy of Sciences, Beijing 100049, China

⁵Center for Excellence in Urban Atmospheric Environment, Institute of Urban Environment, Chinese Academy of Sciences (CAS), Xiamen 361021, China

⁶Asia Center for Air Pollution Research (ACAP), 1182 Sowa, Nishi-ku, Niigata, Niigata 950–2144, Japan

⁷Department of Civil and Environmental Engineering, University of Tennessee, Knoxville, TN 37996, USA

⁸Guangdong-Hongkong-Macau Joint Laboratory of Collaborative Innovation for Environmental Quality, Institute for Environment and Climate Research, Jinan University, Guangzhou 510275, China

⁹Graduate School of Maritime Sciences, Kobe University, Kobe, Hyogo 658–0022, Japan

¹⁰National Institute for Environmental Studies (NIES), Tsukuba, Ibaraki 305–8506, Japan

¹¹Faculty of Life and Environmental Sciences, University of Tsukuba, Tsukuba, Ibaraki 305–8572, Japan

¹²Jiangsu Key Laboratory of Atmospheric Environment Monitoring and Pollution Control, Collaborative Innovation Center of Atmospheric Environment and Equipment Technology, School of Environmental Science and Engineering, Nanjing University of Information Science and Technology, Nanjing 210044, China

¹³Research Institute for Applied Mechanics (RIAM), Kyushu University, Kasuga, Fukuoka 816–8580, Japan

¹⁴Ministry of Education Key Laboratory for Earth System Modeling, Department of Earth System Science, Tsinghua University, Beijing 100084, China

¹⁵Center for Global and Regional Environmental Research, University of Iowa, Iowa City, IA 52242, USA

Correspondence: Syuichi Itahashi (isyuichi@criepi.denken.or.jp)

Received: 1 July 2019 – Discussion started: 8 August 2019

Revised: 14 December 2019 – Accepted: 14 January 2020 – Published: 4 March 2020

Abstract. The Model Inter-Comparison Study for Asia (MICS-Asia) phase III was conducted to promote understanding of regional air quality and climate change in Asia, which have received growing attention due to the huge amount of anthropogenic emissions worldwide. This study provides an overview of acid deposition. Specifically, dry and wet deposition of the following species was analyzed: S (sulfate aerosol, sulfur dioxide (SO_2), and sulfuric acid (H_2SO_4)), N (nitrate aerosol, nitrogen monoxide (NO), nitrogen dioxide (NO_2), and nitric acid (HNO_3)), and A (am-

monium aerosol and ammonia (NH_3)). The wet deposition simulated by a total of nine models was analyzed and evaluated using ground observation data from the Acid Deposition Monitoring Network in East Asia (EANET). In the phase III study, the number of observation sites was increased from 37 in the phase II study to 54, and southeast Asian countries were newly added. Additionally, whereas the analysis period was limited to representative months of each season in MICS-Asia phase II, the phase III study analyzed the full year of 2010. The scope of this overview mainly focuses

on the annual accumulated deposition. In general, models can capture the observed wet deposition over Asia but underestimate the wet deposition of S and A, and show large differences in the wet deposition of N. Furthermore, the ratio of wet deposition to the total deposition (the sum of dry and wet deposition) was investigated in order to understand the role of important processes in the total deposition. The general dominance of wet deposition over Asia and attributions from dry deposition over land were consistently found in all models. Then, total deposition maps over 13 countries participating in EANET were produced, and the balance between deposition and anthropogenic emissions was calculated. Excesses of deposition, rather than of anthropogenic emissions, were found over Japan, northern Asia, and southeast Asia, indicating the possibility of long-range transport within and outside of Asia, as well as other emission sources. To improve the ability of models to capture the observed wet deposition, two approaches were attempted, namely, ensemble and precipitation adjustment. The ensemble approach was effective at modulating the differences in performance among models, and the precipitation-adjusted approach demonstrated that the model performance for precipitation played a key role in better simulating wet deposition. Finally, the lessons learned from the phase III study and future perspectives for phase IV are summarized.

1 Introduction

With recent increases in anthropogenic emissions, Asia has experienced the highest atmospheric acid deposition worldwide (Vet et al., 2014). Atmospheric concentrations and deposition are monitored in the US by the Clean Air Status and Trends Network (CASTNET) (CASTNET, 2019) and in Europe by the European Monitoring and Evaluation Programme (EMEP) (EMEP, 2019). Over Asia, the Acid Deposition Monitoring Network in East Asia (EANET) (EANET, 2019a) has been maintaining a regular observation network since 2000 to measure and understand acid deposition in Asia. The detailed findings from EANET have been reported in its first (EANET, 2006a, b), second (EANET, 2011a, b), and third (EANET, 2016a, b) periodic reports and in a scientific review (EANET, 2015). Data are also available to the public (EANET, 2019b).

Atmospheric pollutants and deposition have been shown to be affected not only by local sources but also by long-range transport. Observation is of course important to measure phenomena in the atmosphere at specific sites. However, there is sometimes difficulty in interpreting such phenomena due to the complex impacts of both nearby and distant sources. Chemical transport models (CTMs) representing the fate of atmospheric pollutants from emissions, transport, chemical reactions, and deposition have been recognized as valuable tools for modern atmospheric environmental sci-

ences. Although CTMs are based on state-of-the-art science, their uncertainties should be considered (Carmichael et al., 2008a). An interpretation based on one CTM can cause misunderstanding of phenomena due to its uncertainty. To further our understanding of CTMs over Asia, the Model Inter-Comparison Study for Asia (MICS-Asia) phase I was conducted in 1998–2000 (Carmichael et al., 2002) and MICS-Asia phase II was conducted in 2003–2008 (Carmichael et al., 2008b). Phase I focused on sulfur concentrations and deposition due to long-range transport in January and May 1993. A total of eight Eulerian and Lagrangian models were used. Observation datasets of sulfur dioxide (SO_2) and sulfate aerosol concentrations and wet sulfate aerosol (SO_4^{2-}) deposition were prepared by a cooperative monitoring network in eastern Asia (Fujita et al., 2000), and a total of 18 sites located in China, Taiwan, Republic of Korea, and Japan were compared with models. Estimates of deposition were consistent among different models but varied by a factor of 5 at some locations. The reason for this variability was determined to be emissions and the underlying meteorological field. It was also found that the model structure of vertical resolution was more important than the parameterization used in the chemical conversion and removal processes. MICS-Asia phase II focused on oxidants (Ox) and particulate matter (PM) (Carmichael et al., 2008b). In terms of deposition, the dry deposition of SO_4^{2-} , nitrate (NO_3^-), and ammonium (NH_4^+) aerosol, the relevant gas species SO_2 , nitric acid (HNO_3), and ammonia (NH_3), and the wet deposition of SO_4^{2-} , NO_3^- , and NH_4^+ were compared among eight Eulerian models. To compare the seasonality of deposition, four periods (March, July, and December 2001 and March 2002) were analyzed. The EANET observation data of wet deposition at 37 sites were compared with models (Wang et al., 2008). The models generally reproduced acid deposition in China, Republic of Korea, Japan, and southeast Asia but could not accurately describe deposition in inland areas such as Mongolia and Russia. These differences were attributed to differences in meteorology, chemical mechanisms, and deposition parameterizations. In phase II, the ensemble mean deposition over eastern Asia based on eight models was determined for the first time and showed better skill than any single model. Additionally, in phase II, emission data were made to be uniform to remove potential discrepancies, but participant models used different modeling domains with different horizontal and vertical structures and different meteorological models. Here, we present MICS-Asia phase III. This phase consists of three parts: topic 1, the comparison and evaluation of current multiscale air quality models; topic 2, the development of reliable emission inventories in Asia; and topic 3, the interactions between air quality and climate change. Scientific papers focusing on gas-phase species (Kong et al., 2020), aerosols (Chen et al., 2019), and ozone (O_3) (Akimoto et al., 2019; Li et al., 2019) have been published. The details of topic 2 (Li et al., 2017a) and topic 3 (Gao et al., 2018) have also been reported.

This paper is concerned with topic 1 and focuses on deposition – namely, the output process from the atmosphere together with the input process to the surface. This paper is structured as follows. Section 2 introduces the framework of the model intercomparison study for deposition. Models and observations are, respectively, described in Sect. 2.1 and 2.2. Section 3 is dedicated to results. Section 3.1 presents an evaluation of precipitation, and Sect. 3.2 presents an evaluation of wet deposition. Section 4 provides an in-depth discussion of the analysis results. First, Sect. 4.1 presents total deposition maps over Asia. The proportion of wet deposition to total deposition over Asia was analyzed in order to clarify the relative importance of dry and wet deposition processes. By comparing the amount of anthropogenic emissions that are used as input to the atmosphere, the implications of other emission sources and long-range transport are discussed. Next, in Sect. 4.2, an ensemble approach is applied to combine multi-model results. Then, in Sect. 4.3, a precipitation-adjusted approach is applied with the aim of further improving model performance for simulating wet deposition. Finally, Sect. 5 summarizes this research and puts forward future perspectives for MICS-Asia phase IV.

2 Framework of model intercomparison for deposition

2.1 Model description

In MICS-Asia phase III, all participating models were run for the year 2010 and requested to submit simulations of the monthly accumulated amounts of dry and wet deposition of S species (sulfate aerosol, SO_2 , H_2SO_4), N species (nitrate aerosol, NO, NO_2 , HNO_3), and A species (ammonium aerosol and NH_3). A total of nine models (M1, M2, M4, M5, M6, M11, M12, M13, and M14; these numbers are unified in MICS-Asia phase III activities) were used in this deposition analysis. These models and their configurations are summarized in Table 1. This study used four different CTMs: the Community Multiscale Air Quality (CMAQ) modeling system (Byun and Schere, 2006), developed by the US Environmental Protection Agency (EPA); the nested air quality prediction model system (NAQPMS), developed by the Institute of Atmospheric Physics (IAP) of the Chinese Academy of Sciences (CAS) (Wang et al., 2001; Li et al., 2016; Ge et al., 2014); the non-hydrostatic mesoscale model coupled with chemistry transport model (NHM-Chem), developed by the Meteorological Research Institute (MRI) in Japan (Kajino et al., 2018, 2019); and the global three-dimensional model of atmospheric chemistry driven by meteorological input from the Goddard Earth Observing System with chemistry (GEOS-Chem), developed at Harvard University (Bey et al., 2001). Basically, phase III was conducted with a unified domain and meteorological field as a “standard” setting based on experience in phases I and II. The modeling domain covers the whole of Asia with a horizontal grid resolution of

Table 1. Descriptions of the models used in this acid deposition study.

No.	M1	M2	M4	M5	M6	M11	M12	M13	M14
Model (version)	CMAQ (5.0.2)	CMAQ (5.0.2)	CMAQ (4.7.1)	CMAQ (4.7.1)	CMAQ (4.7.1)	NAQPMS	NHM-Chem	GEOSS-Chem (9.1.3)	CMAQ (4.6)
Domain ^a	Standard	Standard	Standard	Standard	Standard	Standard	Standard	Nested Asia	Smaller area in Asia
Meteorological field	WRF	WRF	WRF	WRF	WRF	WRF	WRF	GEOS-5	RAMS
Horizontal advection ^b	Yamo	Yamo	PPM	PPM	Yamo	WA	WA	TPCORE	PPM
Vertical advection ^b	PPM	PPM	PPM	PPM	Yamo	WA	WA	TPCORE	PPM
Horizontal diffusion ^c	Multiscale	Multiscale	Multiscale	Multiscale	Multiscale	BD	Multiscale	HB	Multiscale
Vertical diffusion ^c	ACM2	ACM2	ACM2 (inline)	ACM2 (inline)	ACM2 (inline)	BD	MYJ	HB	ACM2
Gas-phase chemistry ^d	SAPRC-99	SAPRC-99	SAPRC-99	SAPRC-99	SAPRC-99	CBMZ	SAPRC-99	Bey	SAPRC-99
Aerosol chemistry ^e	AERO6	AERO6	AERO5	AERO5	AERO5	Li	Kajino	Park, Pye	AEROS
Thermodynamics ^f	Version 2.1	Version 2.1	Version 1.7	Version 1.7	Version 1.7	Version 1.7	Version 1.7	Version 2.1	Version 1.7
Dry deposition ^g	M3DRY	M3DRY	M3DRY	M3DRY	M3DRY	Wesely	Kajino	Wesely, Wang	M3DRY
Surface layer height	58 m	58 m	58 m	58 m	58 m	48 m	27 m	123 m	100 m
Wet deposition ^h	Foley	Foley	Foley	Foley	Foley	Ge	Kajino	Liu	Foley
Boundary condition ⁱ	GEOS-Chem	Default	CHASER	CHASER	CHASER	CHASER	CHASER	GEOS-Chem	GEOS-Chem

^a “Standard” indicates the unified domain in MICS-Asia phase III. See text for details. ^b References for the advection scheme are as follows: ACM2: Asymmetric Convective Model version 2 (Plein and Chang, 1992; Plein, 2007a, b); BI: Byun and Dennis, 1995; HB: Holtslag and Boville, 1998; TPCORE: Wang et al., 2004. ^c References for the diffusion scheme are as follows: Yamo: Yamartino, 1993; PPM: piecewise parabolic method (Colella and Woodward, 1984); WA: Waclawek and Alekseev, 1998; TPCORE: Bey et al., 2001; CBMZ: Zaveri and Peters, 1999; SAPRC-99: Carter, 2000. ^d References for the gas-phase chemistry are as follows: BEY: Bey et al., 2001; CBMZ: Zaveri and Peters, 1999; SAPRC-99: Carter, 2000. ^e References for the aerosol chemistry are as follows: AEROS: AEROS6: Kajino: Kajino et al., 2018; Li: Li et al., 2011; Park: Park et al., 2009. ^f On thermodynamics. All models use ISORROPIA but different versions, namely version 1.7 (Nenes et al., 1998) or version 2.1 (Fountoukis and Nees, 2007). ^g References for the dry deposition scheme are as follows: M3DRY: Plein et al., 2001; Kajino: Kajino et al., 2018; Wang: Wang et al., 2004; Wesely: Wesely, 1989. ^h References for the wet deposition scheme are as follows: Foley: Foley et al., 2010; Ge: Ge et al., 2014; Kajino: Kajino et al., 2018; Liu: Liu et al., 2001. ⁱ References for the boundary condition are as follows: CHASER: Sudo et al., 2002a, b; GEOS-Chem: Bey et al., 2001. Note that model M2 adopted the default boundary condition in the Community Multiscale Air Quality (CMAQ) modeling system.

45 km by 182×172 grids on a Lambert conformal projection, as shown in Fig. 1, and with 40 vertical layers from the surface to 10 hPa. The meteorological fields were driven by the Weather Research and Forecasting (WRF) model version 3.4.1 (Skamarock et al., 2008). Analysis nudging was conducted using the National Centers for Environmental Prediction and National Center for Atmospheric Research (NCEP/NCAR) final analysis data (FNL) (NCEP/NCAR, 2020), available with a $1^\circ \times 1^\circ$ horizontal resolution and 6 h temporal resolution for temperature, wind, and water vapor. For this deposition analysis, seven of the nine models (M1, M2, M4, M5, M6, M11, and M12) were configured with the same domain and meteorological conditions driven by the WRF. The WRF is configured as follows: longwave radiation is computed with the rapid radiative transfer model (Mlawer et al., 1997), shortwave radiation with the Goddard scheme (Chou and Suarez, 1994; Matsui et al., 2018), microphysics with Lin's scheme (Chen and Sun, 2002), cumulus physics with the Grell 3D ensemble scheme (Grell, 1993; Grell and Devenyi, 2002), the planetary boundary layer with the Yonsei University scheme (YSU) (Hong et al., 2006), the surface layer with the revised fifth-generation Penn State/NCAR Mesoscale Model (MM5) (Jiménez et al., 2012), and land surface with the unified Noah model (Tewari et al., 2004). The WRF also includes the urban canopy model (Chen et al., 2011). One model (M13) was configured with a horizontal grid resolution of $0.5^\circ \times 0.667^\circ$ covering part of Asia (11°S – 55°N , 70 – 150°E) with 47 vertical layers from the surface to 0.01 hPa. This model's meteorological fields were driven by the assimilated meteorological fields from the Goddard Earth Observing System 5 (GEOS-5) of the US National Aeronautics and Space Administration (NASA) (NASA, 2020). Another model (M14) covered a smaller domain compared with the “standard”, with a horizontal grid resolution of 45 km and 15 vertical layers. The meteorological fields for this model were simulated by the Regional Atmospheric Modeling System (RAMS) (Pielke et al., 1992) using FNL for analysis nudging as in the “standard” WRF simulation. As input data, emissions were unified for all models. The anthropogenic emissions over Asia were taken from the MIX anthropogenic emission inventory developed for MICS-Asia phase III (Li et al., 2017a). This inventory was developed by harmonizing emission inventories over Asia using a mosaic approach. The base inventory was the Regional Emission Inventory in Asia (REAS) version 2.1 (Kurokawa et al., 2013), with replacement over China using the Multi-Resolution Emission Inventory for China (MEIC), developed by Tsinghua University, and a high-resolution NH₃ inventory developed by Peking University (Huang et al., 2012); replacement over the Republic of Korea using the Clean Air Policy Support System (CAPSS) (Lee et al., 2011); replacement over Japan using the Japan Auto-Oil Program (JATOP) (JPEC, 2012a, b, c); and replacement over India using an Indian inventory developed by Argonne National Laboratory (Lu et al., 2011; Lu and Streets, 2012). Based on the WRF meteorological field,

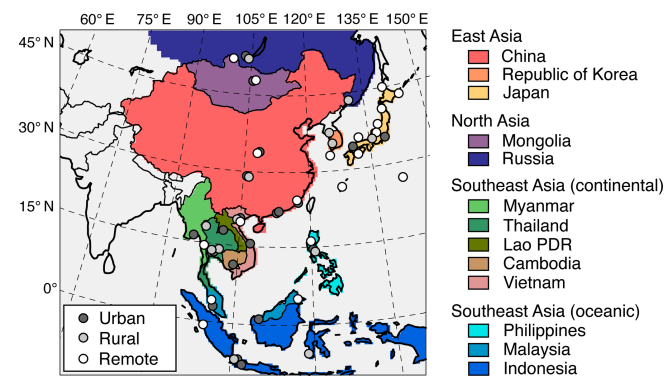


Figure 1. Map of the unified domain of MICS-Asia phase III. Circles with different colors indicate observation sites in remote (white), rural (light gray), and urban (dark gray) areas as classified by the EANET definitions. Map colors indicate the 13 countries participating in EANET in 2010 that were used for the analysis of deposition amount, which were classified into four regions in this study.

hourly biogenic emissions were calculated by the Model of Emissions of Gases and Aerosols from Nature (MEGAN) version 2.04 (Guenther et al., 2006). Emissions from biomass burning were taken from the Global Fire Emission Database (GFED) version 3 (van der Werf et al., 2010). SO₂ emissions from volcanoes were obtained from the AEROCOM program (AEROCOM, 2019). These emissions were unified and provided as an input dataset, and the temporal variation and vertical allocation were requested to follow the setup table; however, there seems to have been a mismatch during their process for each model. For example, the differences in NO emissions intensity were reported in our companion paper focusing on O₃ analysis (Li et al., 2019). In this sense, phase III was conducted not as a model intercomparison but rather as a modeling system intercomparison. This is one of the lessons learned from the phase III study and one of our future research subjects to provide a single model-ready emission file; however, this can propose the potential model variation caused by the setup of the modeling system.

The models used for this deposition analysis were configured with various physical (advection and diffusion scheme) and chemical (gas and aerosol chemistry) processes. The physical model setup for horizontal and vertical advection and diffusion processes was based on their CTM, and CMAQ provides some options to choose them; hence, setups are different even in the same model version. In the chemical scheme, gas-phase chemistry was configured by SAPRC-99 (Carter et al., 2000) to treat 76 species with 214 reactions for M1, M2, M4, M5, M6, M12, and M14; CBMZ (Zaveri and Peters, 1999) including 67 species and 164 reactions for M11; and the developed scheme in GEOS-Chem (Bey et al., 2001) constructed with 80 species and 300 chemical reactions for M13. Aerosol treatment in the models was AERO5 or AERO6 in CMAQ models M1, M2, M4, M5, M6, and

M14, and the representations of secondary organic aerosol (SOA) in these are, respectively, documented in their evaluation documents for AERO5 (Carlton et al., 2010) and AERO6 (Simon and Bhate, 2012). A bulk yield scheme to treat six SOAs has been embedded in M11 (Li et al., 2011). The unique options for aerosol representations with five-category non-equilibrium, three-category non-equilibrium, and bulk equilibrium for research on climate, air pollution, and operational forecasts were available in M12, and details have been reported elsewhere (Kajino et al., 2018, 2019). The originally developed scheme for M13 in GEOS-Chem is available in the literature (Park et al., 2004; Pye et al., 2009). Regarding the thermodynamic equilibrium to treat inorganic aerosol species, the ISORROPIA model was used for all models but with different versions, namely, version 1.7 (Nenes et al., 1998) and the updated version (2.1) to further treat trace metals (Fountoukis and Nenes, 2007). CTMs configured the dry deposition process based on the resistance-in-series model (Wesely and Hicks, 1977). Models M11 and M13 were based on the traditional scheme of Wesely (1989), with numerous modifications for M13 (Wang et al., 2004), and CMAQ models M1, M2, M4, M5, M6, and M14 used the M3DRY scheme (Pleim et al., 2001). The dry deposition scheme in M12 was extensively modified to include the updated observation data; details can be found in the description paper (Kajino et al., 2018, 2019). For the wet deposition process, theoretically, all models use Henry's law to entrain the air pollutants into clouds. The sequential wet deposition process and related aqueous-phase chemistry were based on the Regional Acid Deposition Model (RADM) (Chang et al., 1987). In the case of CMAQ, there is an improvement in the treatment of the precipitation flux before and after the release of version 4.7 (Foley et al., 2010). CMAQ uses an algorithm to allocate precipitation amounts to individual layers based on a normalized profile of hydrometeorological components of rain, snow, and graupel. Before version 4.7, CMAQ allocated the precipitation flux into vertical layers without taking into account the layer thickness; hence, many air pollutants were removed from thin layers but fewer air pollutants were removed from thick layers. In version 4.7, this point was revised to compute the precipitation flux for each layer as a function of the non-convective precipitation, the sum of hydrometers, and the layer thickness. This difference might be found in M14 and other CMAQ models; however, the input meteorological data are different for RAMS and WRF, and it is difficult to detect the effect of this difference. A similar approach with CMAQ is also taken in M11. The details of wet deposition processes are described in the description papers for model M12 (Kajino et al., 2018, 2019). The wet deposition scheme in M13 has been tested through the combined use of terrigenic ^{210}Pb and cosmogenic ^7Be (Liu et al., 2001). MICS-Asia phase III provides two sets of lateral boundary conditions derived from the 3-hourly global model outputs of GEOS-Chem (Bey et al., 2001) and CHASER (Sudo et al., 2002a, b); GEOS-Chem was run with $2.5^\circ \times 2^\circ$ resolution and

47 vertical layers and CHASER was run with $2.8^\circ \times 2.8^\circ$ resolution and 32 vertical layers, and the participants were able to choose between them. Models M1, M13, and M14 used GEOS-Chem, and models M4, M5, M6, M11, and M12 used CHASER. Model M2 used the default boundary condition field provided in the CMAQ modeling system.

2.2 EANET observations

In this overview paper, model evaluations are based on EANET observations over Asia. In EANET, wet deposition is measured by a wet-only sampler designed to collect precipitation samples during rainfall. The locations of observation sites are shown in Fig. 1. Table 2 lists detailed information including latitude, longitude, altitude (meters above sea level; m.a.s.l.), and the classification, sampling interval, and analysis method for anions and cations at each site. In EANET, site classification is defined as follows: urban sites are defined as urbanized and industrial areas or the areas immediately outside them; rural areas are defined as those more than 20 km away from large pollution sources; and remote areas are defined as those more than 50 km away from large pollution sources and more than 500 m away from main roads. The sampling intervals were different from site to site, and a monthly accumulated dataset was used for the model evaluation. The analysis method for anions (SO_4^{2-} and NO_3^-) and cations (NH_4^+) was based on ion chromatography at most sites, with some exceptions in Russia (see Table 2). The observed data were checked by ion balance and conductivity agreement, and the completeness of the data was determined from the duration of precipitation coverage and total precipitation amount. More details can be found in EANET manuals (EANET, 2000, 2010a).

To compare and evaluate the model simulation results with EANET observations, we used the statistical metrics of correlation coefficient (R), normalized mean bias (NMB), and normalized mean error (NME), which are defined as follows:

$$R = \frac{\sum_1^N |(O_i - \bar{O})(M_i - \bar{M})|}{\sqrt{\sum_1^N (O_i - \bar{O})^2} \sqrt{\sum_1^N (M_i - \bar{M})^2}} \quad (1)$$

$$\text{NMB} = \frac{\sum_1^N (M_i - O_i)}{\sum_1^N O_i} \quad (2)$$

$$\text{NME} = \frac{\sum_1^N |M_i - O_i|}{\sum_1^N O_i}. \quad (3)$$

Here, N is the total number of paired observations (O) and models (M). Furthermore, in order to judge the agreement between simulation and observation, the percentages within a factor of 2 (FAC2) and within a factor of 3 (FAC3) were also calculated.

For the analysis of the total amount of deposition over Asia, 13 countries in Asia participating in EANET activities were targeted, as shown in Fig. 1. These 13 countries were divided into four regions: east Asia (China, Republic of

Table 2. Locations and methodology for 54 EANET observation sites.

No.	Country	Name	Latitude (°)	Longitude (°)	Altitude (m a.s.l.)	Classification	Sampling interval	Anion analysis	Cation analysis
1	China	Zhuxiandong	22.20	113.52	45	Urban	Daily	IC	IC
2		Xiang Zhou	22.27	113.57	40	Urban	Daily	IC	IC
3		Hongwen	24.47	118.13	50	Urban	Daily	IC	IC
4		Xiaoping	24.85	118.03	686	Remote	Daily	IC	IC
5		Haifu	29.62	106.50	317	Urban	Daily	IC	IC
6		Jinyunshan	29.82	106.37	262	Rural	Daily	IC	IC
7		Shizhan	34.23	108.95	400	Urban	Daily	IC	IC
8		Jiwozi	33.83	108.80	1800	Remote	Daily	IC	IC
9	Republic of Korea	Cheju	33.30	126.16	72	Remote	Daily	IC	IC
10		Imsil	35.60	127.18	205	Rural	Daily	IC	IC
11		Kanghwa	37.70	126.28	150	Rural	Daily	IC	IC
12	Japan	Hedo	26.87	128.25	60	Remote	Daily	IC	IC
13		Ogasawara	27.09	142.22	230	Remote	Daily	IC	IC
14		Yusuhara	33.38	132.93	790	Remote	Daily	IC	IC
15		Banryu	34.68	131.80	53	Urban	Weekly	IC	IC
16		Oki	36.29	133.19	90	Remote	Daily	IC	IC
17		Ijira	35.57	136.69	140	Rural	Weekly	IC	IC
18		Tokyo	35.69	139.76	26	Urban	Daily	IC	IC
19		Happo	36.70	137.80	1850	Remote	Daily	IC	IC
20		Sado-seki	38.25	138.40	136	Remote	Daily	IC	IC
21		Tappi	41.25	140.35	106	Remote	Daily	IC	IC
22		Rishiri	45.12	141.21	40	Remote	Daily	IC	IC
23		Ochiishi	43.16	145.50	49	Remote	Daily	IC	IC
24	Mongolia	Ulaanbaatar	47.90	106.82	1282	Urban	Daily	IC	IC
25		Terelj	47.98	107.48	1540	Remote	Daily	IC	IC
26	Russia	Mondy	51.67	101.00	2000	Remote	Daily	IC	SP
27		Listvyanka	51.85	104.90	700	Rural	Daily	IC	SP
28		Irkutsk	52.23	104.25	400	Urban	Daily	IC	SP
29		Primorskaya	43.70	132.12	84	Rural	Daily	SP, TI, NP	SP
30	Myanmar	Yangon	16.50	96.12	22	Urban	Daily	IC	IC
31	Thailand	Bangkok	13.77	100.53	2	Urban	Daily	IC	IC
32		Samutprakarn	13.73	100.57	2	Urban	Daily	IC	IC
33		Pathumthani	14.03	100.77	2	Rural	Daily	IC	IC
34		Khanchanaburi	14.77	98.58	170	Remote	Daily	IC	IC
35		Nakhon Ratchasima	14.45	101.88	418	Rural	Daily	IC	IC
36		Chiang Mai	18.77	98.93	350	Rural	Daily	IC	IC
37	Lao PDR	Vientiane	17.00	102.00	177	Urban	Daily	IC	IC
38	Cambodia	Phnom Penh	11.55	104.83	10	Urban	Weekly	IC	IC
39	Vietnam	Da Nang	16.04	108.21	60	Urban	10 d	IC	IC
40		Hanoi	21.02	105.85	5	Urban	Weekly	IC	IC
41		Hoa Binh	20.82	105.33	23	Rural	Weekly	IC	IC
42		Cuc Phuong	20.25	105.72	155	Remote	10 d	IC	IC
43	Philippines	Metro Manila	14.63	121.07	54	Urban	Weekly	IC	IC
44		Los Baños	14.18	121.25	35	Rural	Weekly	IC	IC
45		Mt. Sto. Tomas	16.42	120.60	1500	Rural	Weekly	IC	IC
46	Malaysia	Petaling Jaya	3.10	101.65	87	Urban	Weekly	IC	IC
47		Tanah Rata	4.47	101.38	1470	Remote	Weekly	IC	IC
48		Kuching	1.48	110.47	22	Urban	Weekly	IC	IC
49		Danum Valley	4.98	117.85	427	Remote	Weekly	IC	IC
50	Indonesia	Kototabang	-0.20	100.32	864	Remote	Weekly	IC	IC
51		Jakarta	-6.18	106.83	7	Urban	Weekly	IC	IC
52		Bandung	-6.90	107.58	743	Urban	Daily	IC	IC
53		Serpong	-6.25	106.57	46	Rural	Daily	IC	IC
54		Maros	-4.92	119.57	11	Rural	Weekly	IC	IC

IC: ion chromatography; SP: spectrophotometry; TI: titration; NP: nephelometry.

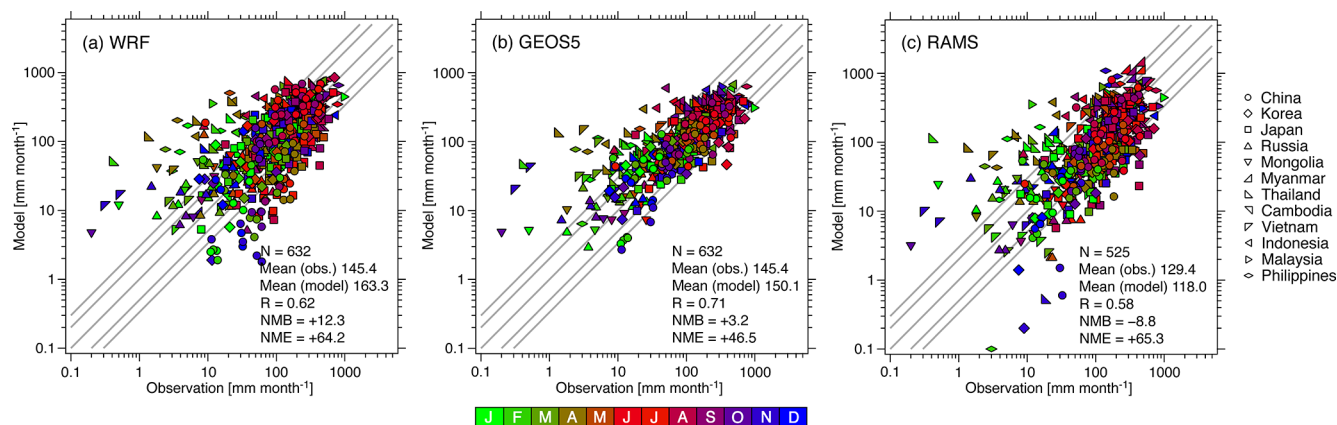


Figure 2. Scatter plots of monthly precipitation amount over Asia simulated by (a) the Weather Research and Forecasting (WRF) model, (b) the Goddard Earth Observing System 5 (GEOS-5) model, and (c) the Regional Atmospheric Modeling System (RAMS) model. Symbols indicate different countries and colors indicate different months. Statistical analysis of the mean, correlation coefficient (R), normalized mean bias (NMB), and normalized mean error (NME) is shown in the inset.

Korea, and Japan); north Asia (Mongolia and Russia), continental southeast Asia (Myanmar, Thailand, Lao People's Democratic Republic (PDR), Cambodia, and Vietnam); and oceanic southeast Asia (the Philippines, Malaysia, and Indonesia).

3 Results

3.1 Evaluation of precipitation

In MICS-Asia phase III, the meteorological field was simulated by WRF for models M1, M2, M4, M5, M6, M11, and M12, by GEOS-5 for model M13, and by RAMS for model M14. Before the evaluation of wet deposition, here, we evaluated the precipitation amount based on the monthly accumulated value. Precipitation data were also taken from EANET observation sites. Figure 2 shows scatter plots of monthly accumulated precipitation amount between observation and models (WRF, GEOS-5, and RAMS), with different symbols for different countries and different colors for different months. For WRF, modeled precipitation slightly overestimated the observed precipitation amount, NMB was +12.3 %, and NME was +64.2 % with an R of 0.62. An overestimation of precipitation by more than a factor of 3 can be found for southeast Asian countries in wintertime and an underestimation of precipitation by more than a factor of 3 can be found in east Asia. For GEOS-5, the agreement with observation was better than for WRF; in particular, there was less model underestimation with GEOS-5 but the overestimation for southeast Asian countries in wintertime was similar for both GEOS-5 and WRF. The statistical performance was as follows: R of 0.71, NMB of +3.2 %, and NME of +46.5 %. For RAMS, due to its smaller domain compared with WRF, the observation number was small; it did not contain data over Malaysia or Indonesia. In contrast

to WRF and GEOS-5, RAMS showed a general underestimation, with NMB of -8.8 %. The R and NME values of RAMS were comparable with those of WRF. In summary, the monthly accumulated precipitation amounts were captured overall by three different meteorological models. However, it should be noted that overestimation (underestimation) could lead to the overestimation (underestimation) of wet deposition. In relation to this point, we applied a precipitation-adjusted approach within the framework of MICS-Asia phase III; this is discussed in Sect. 4.3.

3.2 Evaluation of wet deposition

3.2.1 Wet deposition of S

A comparison of model performance for each of the 54 EANET observation sites is shown in Fig. 3a and a statistical analysis based on monthly accumulated wet deposition is summarized in Table 3. The available numbers for this comparison are smaller compared with the precipitation data (Fig. 2 inset) due to the small number of observations after the quality checking and assurance process. Compared with EANET observation over Asia, it was found that the models tended to underestimate the wet deposition of S, except model M11. Regarding statistical scores, values of R were around 0.4, values of NMB were around -30 %, except for model M11, and values of NME were around 70 %, except for model M11. For model M11, the value of NMB was +44.3 % and that of NME was +136.1 %, showing the overestimation of wet deposition of S, in contrast to other models. The performance of CMAQ models M1, M2, M4, M5, and M6 was similar. The R scores were higher in models M13 and M14 than in other models; these two models were driven by different meteorological models. The underestimation of wet deposition by model M14 was greater than that by the other models, which partly stemmed from the underestima-

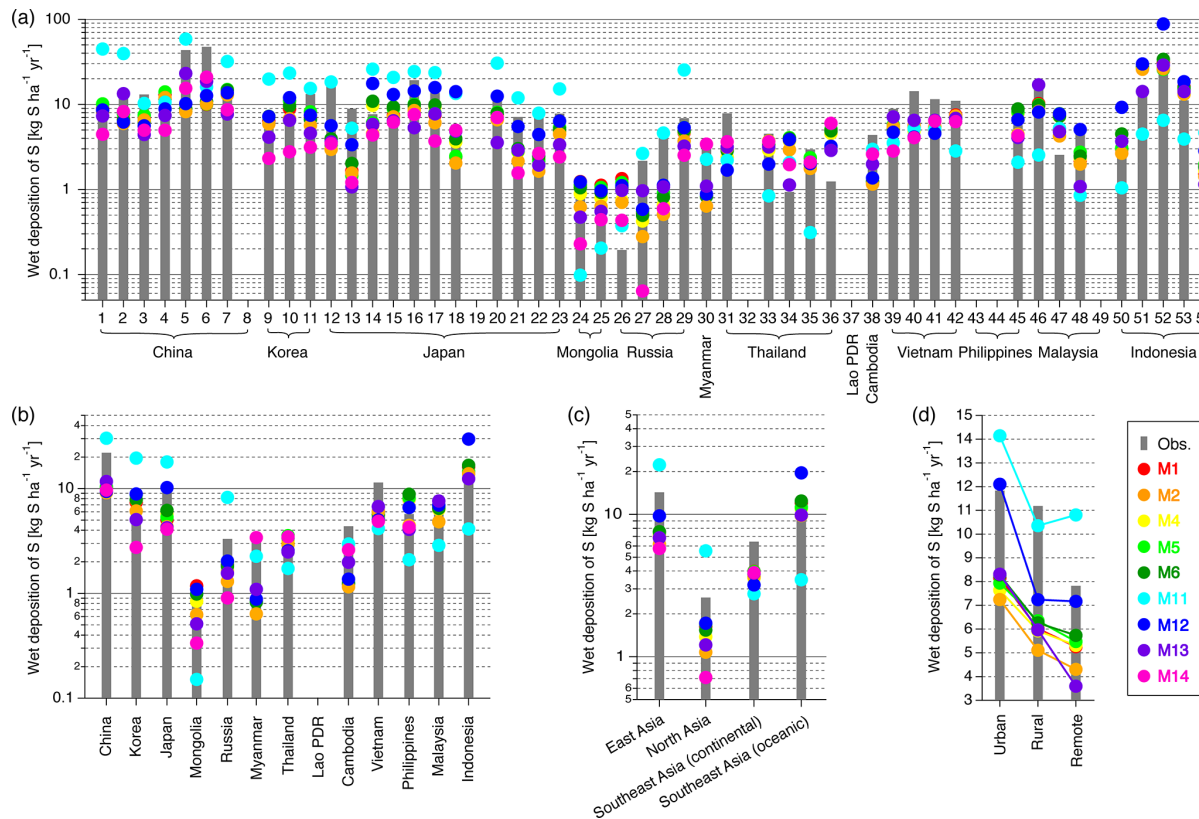


Figure 3. Model evaluation of the annual accumulated wet deposition of sulfate aerosol, sulfur dioxide (SO_2), and sulfuric acid (H_2SO_4) (S) (a) at each EANET observation site, (b) for countries, (c) over four defined regions, and (d) over different site classifications.

tion of precipitation (Sect. 3.1). Approximately 40 % of the model simulation results were within FAC2 and 60 % were within FAC3. For model M11, about 30 % and 40 % of simulation results were within FAC2 and FAC3, respectively.

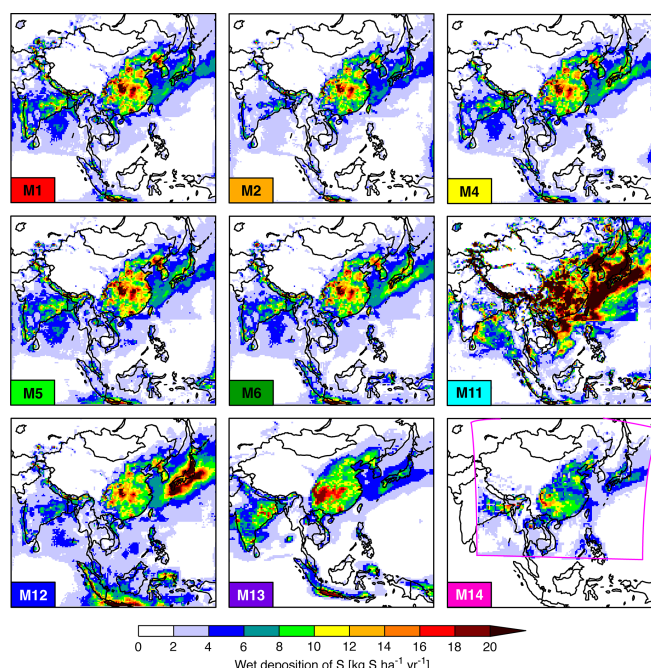
The model performance for atmospheric concentrations was presented in our companion paper (Figs. 3 and 5 and Table 2 of Chen et al., 2019). For consistency with that companion paper, we also performed the model evaluation at the same sites used for the analysis of atmospheric concentrations. The results are shown in Table S1 and the correspondence between the NMB of atmospheric concentration and wet deposition is shown in Fig. S1a. The modeling performance was generally similar for the wet deposition of S using all data (Table 3) and using limited data (Table S1). Models M1, M2, M4, M5, M6, and M13 underestimated atmospheric concentrations of SO_4^{2-} over Asia, with an NMB of around -30% to -20% (Table S1), and accordingly these models also underestimated the wet deposition of SO_4^{2-} . Only models M12 and M14 overestimated atmospheric concentrations of SO_4^{2-} , and model M14 was also distinguished by the overestimation of the atmospheric concentration of SO_4^{2-} over coastal regions, such as over the Korean Peninsula and Japan. Model M11 was the only model to overestimate the wet deposition of SO_4^{2-} and produced the largest underestimation

of the atmospheric concentration of SO_4^{2-} , with an NMB of -34.5% . These overestimations (underestimations) of the atmospheric concentration of SO_4^{2-} are closely related to the underestimation (overestimation) of wet deposition of S found in models M11, M12, and M14. The close relationship between atmospheric concentration and wet deposition was also observed in a model intercomparison study in Japan (Itahashi et al., 2018c). The atmospheric concentration of SO_4^{2-} was underestimated, especially in winter (Fig. 5 of Chen et al., 2019). Another companion paper (Tan et al., 2019) investigated the sulfur oxidation ratio, which represents the conversion rate from SO_2 to SO_4^{2-} . The observation-based ratio was 0.25. Models M1 and M13 both predicted a comparable sulfur oxidation ratio of 0.26; however, models M2, M4, M5, and M6 underestimated the ratio, giving values of around 0.16–0.20, suggesting the insufficient oxidation from the precursor of SO_2 (Fig. 2 of Tan et al., 2019). The sulfur oxidation ratio was strongly underestimated by model M11, which gave a value of 0.12. This underestimation can be corrected by refining the treatment of catalysis using O_2 , introducing the aqueous-phase production of SO_4^{2-} using NO_2 or newly established gas-phase oxidation by the stabilized Criegee intermediate (Itahashi et al., 2018b, c, 2019). Moreover, another study pointed out that heterogeneous chemistry

Table 3. Summary of statistical analysis of model performance for the wet deposition of S.

Model	M1	M2	M4	M5	M6	M11	M12	M13	M14
<i>N</i>				588					
Mean (observation) ($\text{g S ha}^{-1} \text{ month}^{-1}$)				876.5					
Mean (model) ($\text{g S ha}^{-1} \text{ month}^{-1}$)	596.6	510.1	583.0	606.4	624.5	1264.9	808.4	516.6	386.1
<i>R</i>	0.43	0.46	0.44	0.43	0.44	0.34	0.35	0.63	0.56
NMB (%)	-31.9	-41.8	-33.5	-30.8	-28.8	+44.3	-7.8	-41.1	-55.5
NME (%)	+67.7	+66.7	+66.9	+68.4	+67.5	+136.1	+82.1	+58.4	+68.3
FAC2 (%)	40.0	39.3	41.0	40.1	42.3	29.8	39.6	44.9	38.6
FAC3 (%)	60.5	61.4	60.7	60.2	62.6	42.5	59.0	64.8	55.1

Note: models M1, M2, M4, M5, M6, M11, and M12 were based on the unified meteorological field of WRF. Model M13 was based on a different meteorological model (GEOS-5), and the covered domain was also different (see Fig. 4). Model M14 was based on a different meteorological model (RAMS), and the covered domain was also smaller (see Fig. 4).

**Figure 4.** Spatial distributions of the annual accumulated wet deposition of S.

is a possible explanation for the missing production of SO_4^{2-} in models (Zheng et al., 2015; Shao et al., 2019). The modeled sulfur oxidation ratios of models M12 and M14 were 0.33 and 0.57, respectively; that is, the ratios were overestimated. This overestimation is one reason for the overestimation of the atmospheric concentration of SO_4^{2-} by models M12 and M14. In summary, the model performance of M11, M12, and M14 for the overestimations (underestimations) of atmospheric concentration of SO_4^{2-} is characterized by a close relation to the underestimation (overestimation) of wet deposition of S; meanwhile, models M1, M2, M4, M5, M6, and M13 underestimated both atmospheric concentration and wet deposition of S.

The spatial distribution of the wet deposition of S in the present study is displayed in Fig. 4. Model results showed the highest amount of wet deposition (dark red, over $20 \text{ kg S ha}^{-1} \text{ yr}^{-1}$) over eastern China and the island of Java, Indonesia, and moderately high amounts (yellow to orange, $10\text{--}20 \text{ kg S ha}^{-1} \text{ yr}^{-1}$) over the Korean Peninsula, Japan and surrounding oceans, and India. A comparison of the model performance for 13 countries is shown in Fig. 3b. Based on EANET observations, China had the highest amount of wet deposition, with $21.9 \text{ kg S ha}^{-1} \text{ yr}^{-1}$, followed by Indonesia, with $12.4 \text{ kg S ha}^{-1} \text{ yr}^{-1}$, Vietnam, with $11.4 \text{ kg S ha}^{-1} \text{ yr}^{-1}$, and Japan, with $10.6 \text{ kg S ha}^{-1} \text{ yr}^{-1}$. In other countries, the amount of wet deposition of S was below $10 \text{ kg S ha}^{-1} \text{ yr}^{-1}$. Compared with EANET observation data, all the models except M11 underestimated wet deposition in China, whereas M11 overestimated it. The model performance for China was similar to that for the Republic of Korea and Japan. For Indonesia, wet deposition was underestimated by model M11 and overestimated by M12, while the estimations of the other models were comparable to the observed values. Conversely, model M11 overestimated wet deposition in east Asia but performed similarly in Vietnam and other southeast Asian countries to how it did for Indonesia. As summarized in Fig. 3c, model M11 overestimated wet deposition over east and north Asia and underestimated it over southeast Asia. Other models exhibited underestimation over east and north Asia and continental southeast Asia. The wet deposition over oceanic southeast Asia was well captured by all models except M11 and M12, with M12 showing overestimation. The model performance divided into three EANET classifications is also shown in Fig. 3d. The observation results showed a wet S deposition of 11.8 , 11.2 , and $7.8 \text{ kg S ha}^{-1} \text{ yr}^{-1}$ at urban, rural, and remote sites, respectively. This result demonstrates the similarly polluted wet deposition status of urban and rural EANET sites. All models showed a strong decrease in wet deposition at urban sites compared with rural sites but a weak decrease in wet deposition between remote and rural sites. However, since the definition of rural areas is those more than 20 km away from large pollution sources, the hori-

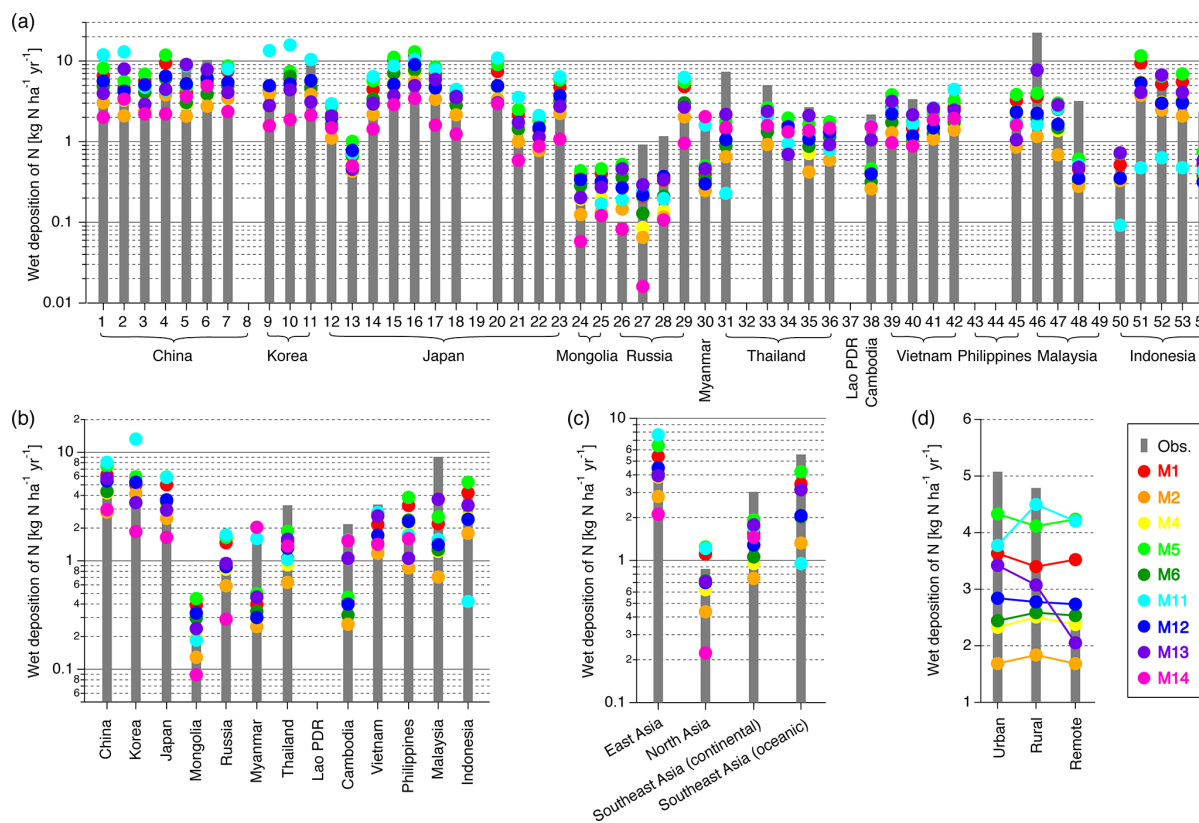


Figure 5. Model evaluation of the annual accumulated wet deposition of nitrate aerosol, nitrogen monoxide (NO), nitrogen dioxide (NO₂), and nitric acid (HNO₃) (N) (a) at each EANET observation site, (b) for countries, (c) over four defined regions, and (d) over different site classifications.

zontal resolution of 45 km has difficulty fully capturing these spatial scales; therefore, a finer-scale simulation will be of interest in a future study.

3.2.2 Wet deposition of N

The model performance for the wet deposition of N was compared with EANET observations; the results for each EANET observation site are shown in Fig. 5a. The model performance for the wet deposition of N exhibited larger variation among models compared with the wet deposition of S. Even in the same model of CMAQ, models M1, M2, M4, M5, and M6 showed different performance for the wet deposition of N. A statistical analysis of model performance for the wet deposition of N is presented in Table 4. Compared with EANET observations, models M5 and M11 overestimated the wet deposition of N, with NMB values of +16.5 % and +51.9 %, respectively; model M1 simulated values that are almost comparable, with NMB of -3.4 %; and other models underestimated the wet deposition of N, with negative NMB values; models M4, M6, M12, and M13 showed NMB values of around -30 %, and models M2 and M14 showed NMB values below -50 %. NME values were greater than +50 % for all models. *R* values ranged from 0.32

to 0.42 for all models driven by WRF, while models M13 and M14, which were simulated with a different meteorological field, showed higher *R* values of 0.62 and 0.51, respectively. This feature of higher *R* values for models M13 and M14 is similar to the finding for the wet deposition of S. Approximately 40 % of the model simulation results were within FAC2, and 60 % were within FAC3. Model M13 showed better agreement, with 54.3 % and 70.6 % of its simulation results being within FAC2 and FAC3, respectively.

The model performance for the atmospheric concentration of NO₃⁻ in our companion paper also showed large differences between models (Figs. 3 and 5 and Table 2 of Chen et al., 2019). The model evaluation for the analysis of atmospheric concentrations for N was conducted at the same sites as those for S (Table S1), as shown in Table S2. The correspondence between the NMB of atmospheric concentration and the NMB of wet deposition is shown in Fig. S1b. Models M2, M4, M5, and M6 showed underestimation, whereas models M1, M11, M12, M13, and M14 showed overestimation for the atmospheric concentration of NO₃⁻. Models M1, M2, and M5 showed better performance in terms of NMB (NMBs between -10 % and 10 %) for the atmospheric concentration of NO₃⁻ (Table S2). If both H₂SO₄ and HNO₃ are present, H₂SO₄ preferentially reacts with NH₃, and there-

Table 4. Summary of statistical analysis of model performance for the wet deposition of N.

Model	M1	M2	M4	M5	M6	M11	M12	M13	M14
<i>N</i>	575							482	
Mean (observation) ($\text{g N ha}^{-1} \text{ month}^{-1}$)	347.5							315.2	
Mean (model) ($\text{g N ha}^{-1} \text{ month}^{-1}$)	337.5	153.4	217.4	407.2	229.1	530.8	247.1	256.8	140.6
<i>R</i>	0.35	0.32	0.34	0.34	0.33	0.42	0.38	0.62	0.51
NMB (%)	-3.4	-56.1	-37.8	+16.5	-34.4	+51.9	-29.3	-26.5	-55.7
NME (%)	+80.7	+72.7	+71.5	+90.9	+72.1	+101.9	+68.8	+54.2	+67.6
FAC2 (%)	42.8	31.1	39.1	41.4	40.9	44.2	43.8	54.3	34.9
FAC3 (%)	62.3	50.3	56.0	59.0	58.1	61.9	61.4	70.6	51.0

Note: models M1, M2, M4, M5, M6, M11, and M12 were based on the unified meteorological field of WRF. Model M13 was based on a different meteorological model (GEOS-5), and the covered domain was also different (see Fig. 6). Model M14 was based on a different meteorological model (RAMS), and the covered domain was also smaller (see Fig. 6).

fore NH_4NO_3 is produced only if excess NH_3 is present. The underestimation of the atmospheric concentration of SO_4^{2-} can lead to the overestimation of the atmospheric concentration of NO_3^- . This can explain the performance of models M1, M11, and M13 but not that of models M12 and M14 because they overestimated the atmospheric concentrations of both SO_4^{2-} and NO_3^- . Another companion paper (Tan et al., 2019) revealed that models M12 and M14 also used a higher nitrogen oxidation ratio (i.e., the ratio of oxidation from NO_2 to NO_3^-) than that of other models and observation, in addition to using a higher sulfur oxidation ratio (Fig. 2 of Tan et al., 2019). The higher oxidation capacity in models M12 and M14 is connected to the overestimation of the atmospheric concentration of both SO_4^{2-} and NO_3^- . On the other hand, models M2, M4, M5, and M6 underestimated the atmospheric concentration of both SO_4^{2-} and NO_3^- . These four models (M2, M4, M5, and M6) also had lower nitrogen oxidation ratios (between 0.08 and 0.14) than the observed value of 0.18 (Fig. 2 of Tan et al., 2019). In summary, for the wet deposition of N, all models except M5 and M11 underestimated this parameter; however, the relationship between the wet deposition of N and the atmospheric concentration of N was not obvious, and this point was different from this relationship for S. Because the correlation coefficient for the model performance of the wet deposition of N is lower than that for S, future studies should focus on N and related species in greater detail. Our future companion paper will attempt a detailed analysis of N using an intensive observation network over China (Ge et al., 2020).

The spatial distribution of the wet deposition of N is shown in Fig. 6. With respect to reactive nitrogen (Nr) deposition, a threshold value of $10 \text{ kg N ha}^{-1} \text{ yr}^{-1}$ has been established (e.g., Bleeker et al., 2011). The exceedance of this threshold value (from yellow to orange and red) was different among models. Models M1, M5, and M11 simulated excess Nr deposition over eastern China and the Sea of Japan, while models M4, M6, M12, and M13 simulated more limited areas of excess Nr deposition and models M2 and M14 showed no excess Nr deposition over Asia. A comparison between country

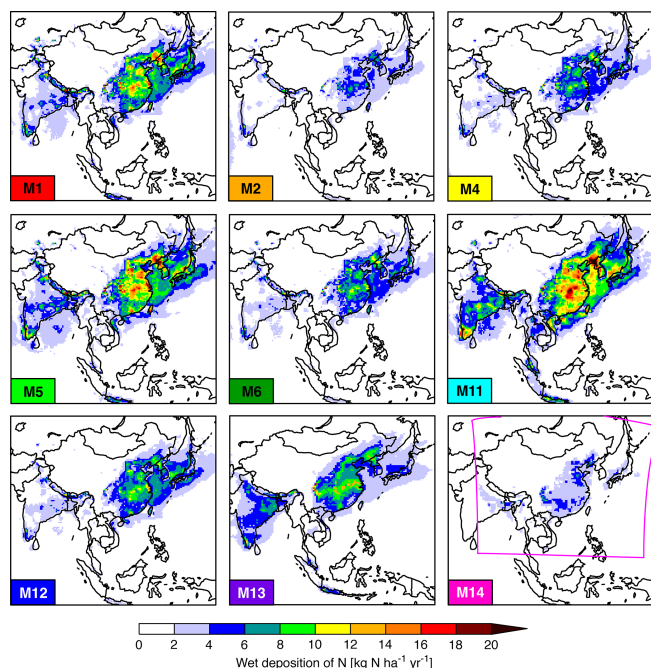


Figure 6. Spatial distributions of the annual accumulated wet deposition of N.

and regional summarized results and EANET observations is shown in Fig. 5b and c. These showed large variability. Over east Asia, the observed wet deposition of N was 6.8, 6.7, and $3.3 \text{ kg N ha}^{-1} \text{ yr}^{-1}$ for China, Republic of Korea, and Japan, respectively, with an average value of $4.9 \text{ kg N ha}^{-1} \text{ yr}^{-1}$. It was also found that models M11, M5, and M1 overestimated and models M14 and M2 underestimated wet deposition. A similar pattern was also observed in north Asia. These results suggest difficulty in the exact estimation of the wet deposition of N and hence in the setting of the threshold value of Nr. Unlike the situation for east and north Asia, all of the models underestimated the wet deposition of N over both continental and oceanic southeast Asian countries. A detailed analysis of site classification was also performed for wet N deposition,

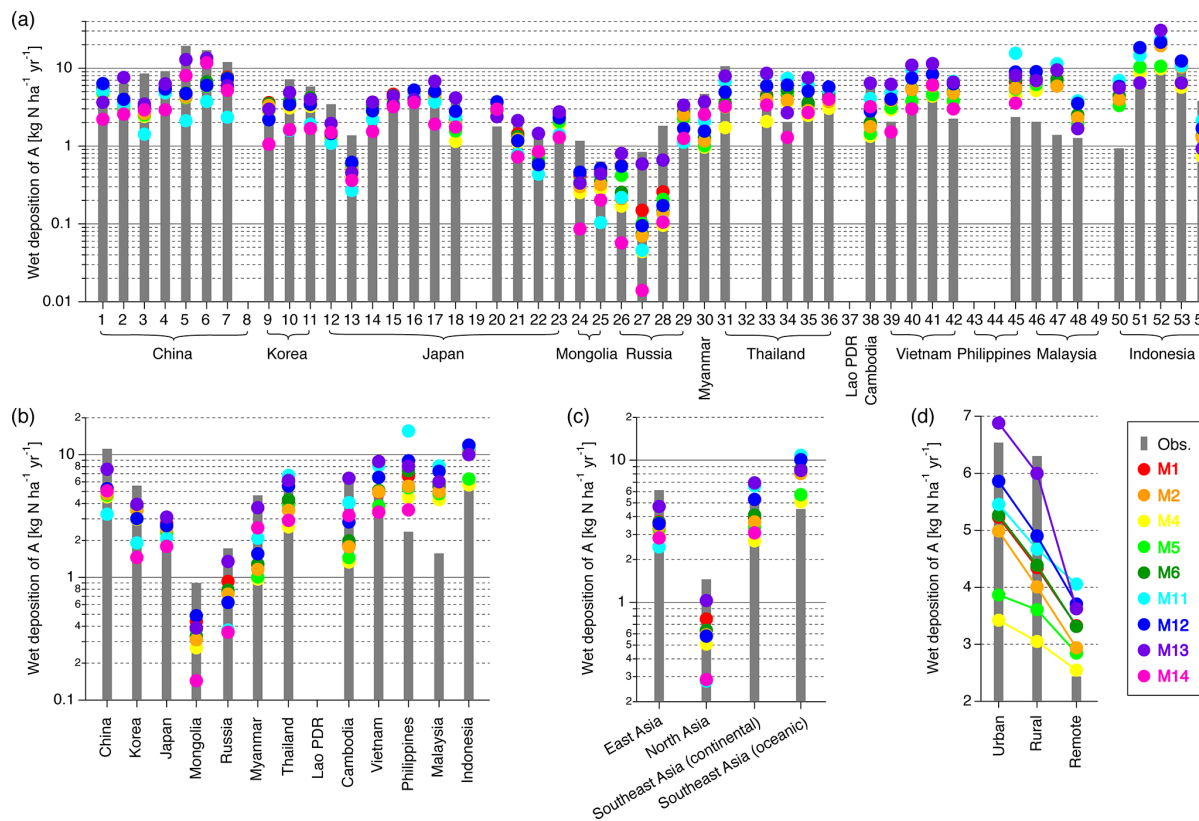


Figure 7. Model evaluation of the annual accumulated wet deposition of ammonium aerosol and ammonia (NH_3) (A) (a) at each EANET observation site, (b) for countries, (c) over four defined regions, and (d) over different site classifications.

as shown in Fig. 5d. Observations indicate a wet deposition of N of 5.2, 4.8, and $2.4 \text{ kg N ha}^{-1} \text{ yr}^{-1}$ at urban, rural, and remote sites, respectively, similar to the findings for the wet deposition of S. Although all models showed underestimation for urban and rural sites, comparable levels of wet deposition over urban and rural sites were simulated by all models. However, the modeled wet N deposition was relatively similar for remote sites and did not reproduce the observed decrease in the wet deposition of N at remote sites compared with rural sites. The exception to this was model M13, which showed a decrease in the wet deposition of N at remote sites compared with rural sites.

3.2.3 Wet deposition of A

Wet deposition of A was compared between model simulations and EANET observations, and the results for observation sites are shown in Fig. 7a. The statistical analyses for the wet deposition of A are listed in Table 5. As NH_4^+ is the counterpart of SO_4^{2-} and NO_3^- , the behavior of the wet deposition of A showed a blend of features of the wet deposition of S and N. In general, model simulations underestimated the wet deposition of A, except model M13. NMB values ranged from -49.3% for model M14 to -0.2% for model M12 to $+8.6\%$ for model M13. NME values were around $+70\%$. R

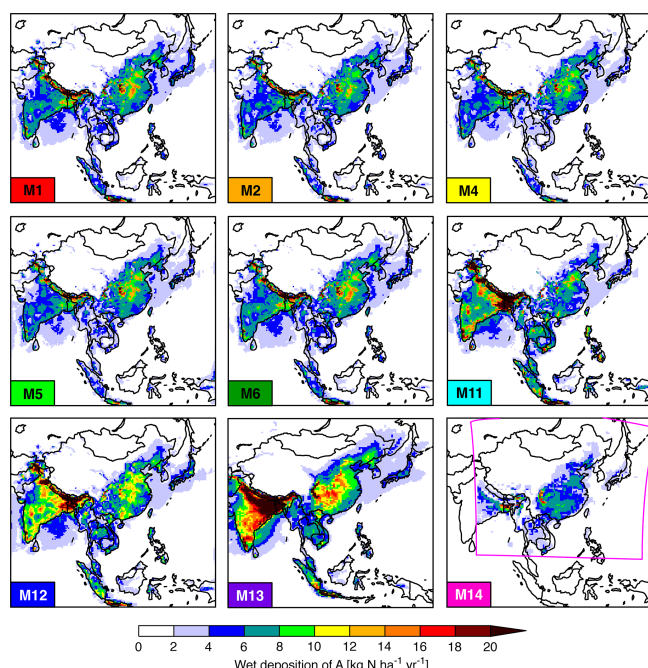
values were around 0.3, while models M13 and M14, which were simulated with a different meteorological field, showed higher R values (0.48 and 0.54, respectively), as was also observed for the wet deposition of S and N. Approximately 40 % of the model simulation results were within FAC2, and less than 60 % were within FAC3. Model M13 showed better agreement, with 50.9 % and 68.3 % of simulation results being within FAC2 and FAC3, respectively.

Our companion paper reported model performance for the atmospheric concentration of NH_4^+ (Figs. 3 and 5 and Table 2 of Chen et al., 2019). The model evaluation for the analysis of atmospheric concentrations for A was conducted at the same sites as those for S and N (Tables S1 and S2), as shown in Table S3, and the correspondence between the NMB of atmospheric concentration and that of wet deposition is shown in Fig. S1c. Generally, the behavior of NH_4^+ is associated with the atmospheric concentrations of SO_4^{2-} and NO_3^- as counterions. The studied models generally underestimated the atmospheric concentration of S and overestimated the atmospheric concentration of N; consequently, all models except M4 overestimated the atmospheric concentration of A. The reason for the different behavior of model M4 is that this model underestimated atmospheric concentrations of NO_3^- . In general, the models overestimated the

Table 5. Summary of statistical analysis of model performance for the wet deposition of A.

Model	M1	M2	M4	M5	M6	M11	M12	M13	M14
<i>N</i>				568					474
Mean (observation) ($\text{g N ha}^{-1} \text{ month}^{-1}$)				440.7					447.0
Mean (model) ($\text{g N ha}^{-1} \text{ month}^{-1}$)	394.7	365.0	278.5	317.7	395.5	433.7	438.7	476.9	225.6
<i>R</i>	0.35	0.36	0.34	0.35	0.35	0.28	0.35	0.48	0.54
NMB (%)	-10.2	-16.9	-36.6	-27.7	-10.0	-1.3	-0.2	+8.6	-49.3
NME (%)	+79.5	+77.7	+75.3	+75.2	+79.9	+92.7	+84.4	+72.1	+68.5
FAC2 (%)	39.6	37.7	35.4	38.4	38.2	31.9	35.9	50.9	35.0
FAC3 (%)	58.5	57.9	53.5	57.6	58.6	48.8	55.5	68.3	54.9

Note: models M1, M2, M4, M5, M6, M11, and M12 were based on the unified meteorological field of WRF. Model M13 was based on a different meteorological model (GEOS-5), and the covered domain was also different (see Fig. 8). Model M14 was based on a different meteorological model (RAMS), and the covered domain was also smaller (see Fig. 8).

**Figure 8.** Spatial distributions of the annual accumulated wet deposition of A.

atmospheric concentration of A and underestimated the wet deposition of A (Fig. S1c); this indicates an inverse relationship between atmospheric concentration and wet deposition processes.

The simulated spatial distribution of the wet deposition of A is displayed in Fig. 8. Compared with the wet deposition of S (Fig. 4) and N (Fig. 6), the wet deposition of A above $2 \text{ kg N ha}^{-1} \text{ yr}^{-1}$ (light blue) was more limited over land. A large amount of wet A deposition (dark red, over $20 \text{ kg N ha}^{-1} \text{ yr}^{-1}$) was found in areas over the central parts of China and India; these areas were simulated to be broader by model M13. The threshold value of Nr deposition of 10 kg N ha^{-1} was found to be exceeded over central China with limited spatial coverage, with model M13 simulating

a broader area. Models M12 and M13 simulated a larger amount of wet A deposition over India and also simulated an extended wet deposition of A from India to the Indian Ocean; however, we cannot judge these simulations due to the lack of observation in this region. The summarized results for countries and regions are shown in Fig. 7b and c. The underestimation of the wet deposition of A over north and east Asia and its overestimation over southeast Asia were consistently observed in models. In particular, all models overestimated the wet deposition of A over the Philippines and Malaysia. These common features across models suggest a shortcoming in the current status model and thus suggest the need to revisit emission inventories. As shown in Fig. 7d, observations showed wet deposition of A of 6.5, 6.3, and $2.4 \text{ kg N ha}^{-1} \text{ yr}^{-1}$ at urban, rural, and remote sites, that is, similar to the observations of the wet deposition of S and N. All models showed a decrease in the wet deposition of A from urban to rural sites and from urban to remote sites, with the decreases being much greater than the observed ones. Despite the underestimation at rural sites, all models overestimated the wet deposition of A at remote sites.

4 Discussion

4.1 Total deposition mapping over Asia

Here, we draw maps of total deposition (defined as the sum of dry and wet deposition) over Asia to investigate the annual accumulated total deposition across various countries and its relation to emission amounts used as input to the atmosphere. In Figs. 9 to 11, the total deposition of S, N, and A over 13 countries participating in EANET is respectively mapped. In each figure, the ensemble mean, which is simply the average of all nine models, is shown in order to demonstrate the spatial distribution pattern. A detailed discussion of the ensemble approach is given in the following (Sect. 4.2). An evaluation of the atmospheric concentrations of gases and aerosols simulated by models is given in our companion papers (Kong et al., 2020; Chen et al., 2019). Due to the diffi-

culty of directly measuring deposition, especially within the framework of observation networks (EANET, 2010b), we relied on model-simulated atmospheric concentrations to estimate amounts of dry deposition. In the Supplement, the annual accumulated dry and total deposition of S, N, and A is, respectively, shown in Figs. S2, S3, S5, S6, and S8 and S9. The components of dry deposition averaged over domain on annual mean are listed in Tables S4 to S6 in the Supplement. In models, SO_2 , HNO_3 , and NH_3 were commonly the most dominant species for dry deposition. To investigate the important processes in S, N, and A deposition, the proportion of wet deposition to total deposition is also illustrated in Figs. S4, S7, and S10, with blue indicating the higher proportion of wet deposition to total deposition and brown indicating the higher proportion of dry deposition to total deposition. As we have seen (e.g., Fig. S1), the underestimation (overestimation) of wet deposition could be related to the overestimation (underestimation) of atmospheric concentration. In terms of dry deposition, which is calculated by multiplying atmospheric concentration and deposition velocity, the underestimation (overestimation) of dry deposition would be directly related to the underestimation (overestimation) of atmospheric concentration. The underestimation (overestimation) of wet deposition can be compensated by the overestimation (underestimation) of dry deposition and may pose the similar total deposition amount. Therefore, this kind of study can give insights into the balance between dry and wet deposition.

In terms of the total deposition of S (Fig. 9), high amounts were seen over east Asian countries: in eastern China to the Korean Peninsula; in Japan and surrounding oceans; in Java, Indonesia; and in eastern India. The total amount of S deposition across China was around $10\,000 \text{ Gg S yr}^{-1}$ ($5600\text{--}15\,500 \text{ Gg S yr}^{-1}$), nearly 10 times more than in the country with the second largest deposition, namely Indonesia, where deposition was around $1300 \text{ Gg S yr}^{-1}$ ($640\text{--}2500 \text{ Gg S yr}^{-1}$). Other countries had total deposition below $1000 \text{ Gg S yr}^{-1}$. The proportions of dry and wet deposition of S are shown in Fig. 9, and the proportion of the wet deposition to the total deposition of S is shown in Fig. S4 in the Supplement. Generally, wet deposition was the most important process in the total deposition of S (e.g., Itahashi, 2018). The proportion of dry deposition was found to be larger over north Asia, and dry deposition was found to be dominant around the Bohai Sea, the Sichuan Basin, and the northwestern boundary of the modeling domain. The proportion of wet deposition to total deposition was higher than 70 % over the ocean. Models M11 and M14 simulated a greater importance of dry deposition, while model M12 simulated a greater importance of wet deposition. Regarding the balance between anthropogenic emissions and deposition amounts, all countries in Asia except China and the Republic of Korea were found to experience a deposition amount that was greater than their own anthropogenic emissions, though with some variability among models. This suggests the existence

of other important sources of emissions, such as volcanic emissions in the case of SO_2 , or the possibility of long-range transport from other countries. It should also be noted that the uncertainty in anthropogenic SO_2 emissions over Asia has been reported to be about $\pm 30\%$ (Kurokawa et al., 2013). For example, for SO_2 , all models estimated more deposition than anthropogenic emissions in Japan. Previous studies based on source–receiver relationships in model experiments indicated the importance of volcanic sources and transboundary air pollution for S over Japan (Kajino et al., 2011; Kuribayashi et al., 2012; Itahashi et al., 2017; Itahashi, 2018). Over north Asia (Mongolia and Russia), all models simulated more deposition than emissions; deposition was predicted to be 1.9 and 2.5 times higher than emissions over Mongolia and Russia, respectively, by model M2, which estimated the lowest total deposition. In north Asia, the long-range transport within the Asian domain and the effect from the northern boundary of modeling domain (i.e., global-scale impacts) are important factors leading to the excess of deposition. Over southeast Asia, although more deposition than emissions was predicted, there was variability between models. Over Myanmar and Cambodia, the estimated anthropogenic SO_2 emissions were low, at 34 and 13 Gg S yr^{-1} , respectively, and all models estimated greater deposition than emissions, suggesting long-range transport from other countries. Over Lao PDR, only model M2 showed comparable values of deposition and emissions, while other models showed an excess of deposition. In Thailand, Vietnam, the Philippines, Malaysia, and Indonesia, some models showed an excess of deposition compared with emissions, while others did not; these results found over southeast Asia indicate the possible importance of long-range transport or other emission sources (e.g., volcanoes and biomass burning). However, this should be carefully interpreted, since the variability of model performance reveals the risk of policymaking relying on the result of only one model.

The map of the total deposition of N (Fig. 10) illustrates a different feature to the map of the total deposition of S (Fig. 9). The total deposition of N is largely limited over land; this is due to the fact that high amounts of dry N deposition are limited to land (Fig. S5). A drastic reduction of the total deposition of N, from over $20 \text{ Gg N ha}^{-1} \text{ yr}^{-1}$ (dark red) to below $10 \text{ Gg N ha}^{-1} \text{ yr}^{-1}$ (green), is found over the eastern coastline of China. The total amount of N deposition over China ranged from 2800 to $7200 \text{ Gg N yr}^{-1}$, with large variability among models. In the other 12 countries, total N deposition was below $1000 \text{ Gg N yr}^{-1}$, thus illuminating the serious N burden over China (Xu et al., 2015). The proportion of wet N deposition to total N deposition is shown in Fig. S7. Over eastern China and other parts of the Asian continent, dry and wet deposition contributed almost equally to the total deposition of N, whereas dry deposition was dominant over western China to the northwestern boundary of China. Over east Asia, from the Korean Peninsula to Japan, the simulated proportion of wet deposition was higher,

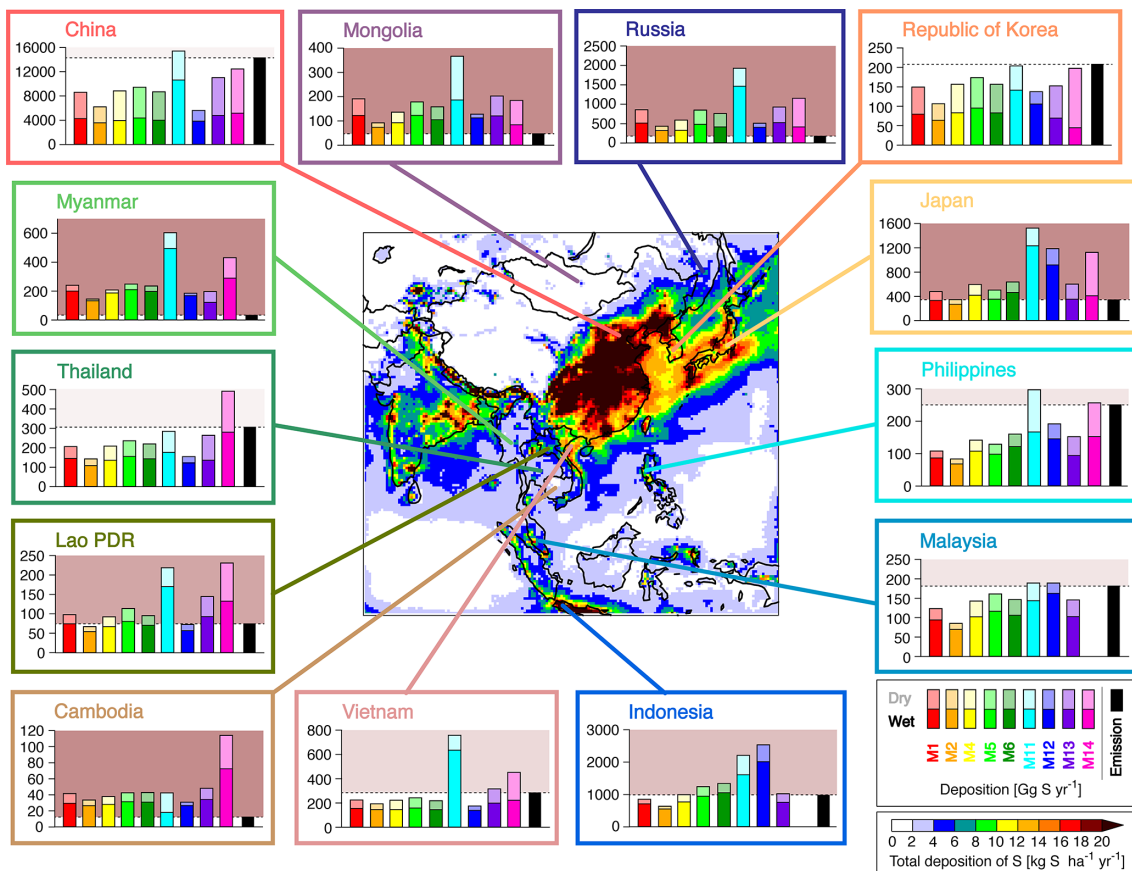


Figure 9. Map of the annual accumulated total S deposition over Asia. The cumulative bar graphs show dry deposition (light colors) and wet deposition (dark colors), with different colors representing different models and black representing the amount of anthropogenic SO₂ emissions. The background red areas of the graphs indicate an excess of total deposition compared to emissions, and their transparency is based on the number of models making this prediction (i.e., bolder colors indicate that more of the nine models simulated the excess).

above 50 %, using models M1, M2, M4, M5, M6, and M13, whereas models M11 and M12 showed predominantly wet deposition, above 70 % and model M14 showed predominantly dry deposition over coastal areas. We note here that the uncertainty in anthropogenic NO_x emissions over Asia has been reported to be about $\pm 40\%$ (Kurokawa et al., 2013). From the perspective of the balance between the deposition and emissions of N, it was illustrated that an excess of deposition was commonly shown over north Asia (Mongolia and Russia) and continental southeast Asia (Myanmar, Lao PDR, and Cambodia). Over these five countries, the amounts of deposition were greater than anthropogenic NO_x emissions by at least 1.5 times. The importance of long-range transport from other countries in Asia, lateral boundaries, especially for north Asia, and biomass burning, especially for southeast Asia, has been suggested. In other countries in southeast Asia, namely Thailand, the Philippines, Malaysia, and Indonesia, a few models estimated a slight excess of N deposition compared with emissions, but most concluded that local sources were responsible for the total deposition of N. In Japan, model discrepancies were large. Some previ-

ous studies have noted the influence of transboundary transport (Morino et al., 2011; Kajino et al., 2013; Itahashi et al., 2016), whereas other studies have estimated smaller impacts (Lin et al., 2008; Ge et al., 2014). Within the framework of MICS-Asia, further study would be needed to investigate the source–receptor relationships.

The analysis of the total deposition of A (Fig. 11) posed the combined results of the total deposition of S (Fig. 9) and N (Fig. 10) due to the ion counterpart. The simulated total deposition of A was highest over China, at 4000–8000 Gg N yr⁻¹, followed by Indonesia, at 900–1600 Gg N yr⁻¹; for other countries, the deposition was below 1000 Gg N yr⁻¹. Again, the deposition surpassed emissions in north Asia, and long-range transport within and outside of Asia was found to be important. Over Japan, model M12 showed a comparable proportion of deposition and emissions, while other models showed an excess of deposition over emissions. Over southeast Asia excluding the Philippines, the possible importance of long-range transport for the total deposition of A is suggested by other results. The contribution of wet deposition to the total deposition of A is

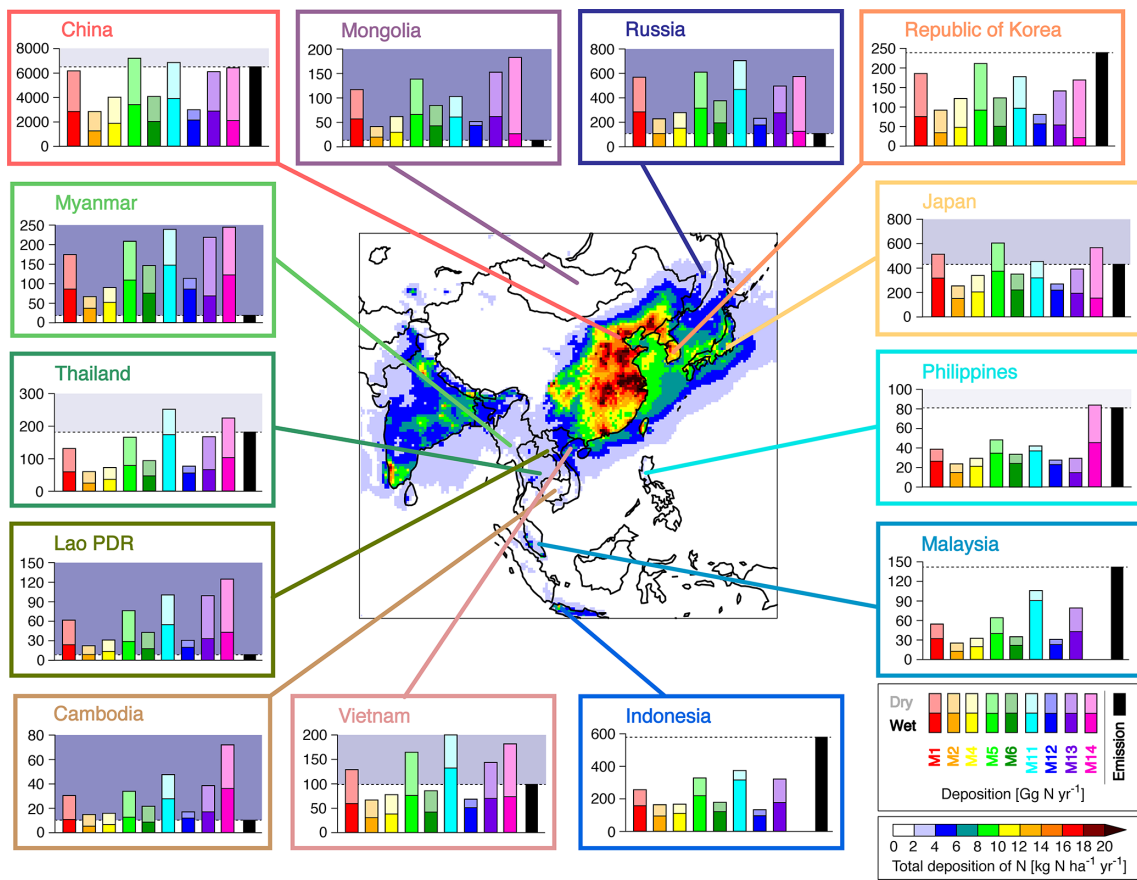


Figure 10. Map of the annual accumulated total N deposition over Asia. The cumulative bar graphs show dry deposition (light colors) and wet deposition (dark colors), with different colors representing different models and black representing the amount of anthropogenic NO_x emissions. The background blue areas of the graphs indicate an excess of total deposition compared to emissions, and their transparency is based on the number of models making this prediction (i.e., bolder colors indicate that more of the nine models simulated the excess).

shown in Fig. S10. The contrast between land and ocean was clearer compared with the proportions of the wet and dry deposition of S and N (Figs. S4 and S7). Over land, the proportion of wet deposition to the total deposition of A was either comparable to or more skewed toward dry deposition than what was found over India and some parts of China and over southeast Asia. In contrast, over ocean, the proportion was above 80 %, demonstrating the importance of the wet deposition of A. Models M11 and M13 showed a lower importance of wet deposition over ocean, with a proportion of 70 % to total deposition. Here, we remind the reader of the performance in southeast Asia (Fig. 7). The analyzed models generally overestimated the wet deposition of A over southeast Asia, and all models significantly overestimated it over the Philippines and Malaysia. By taking into account this model performance, the interpretation of the long-range transport effect will be changed. Compared with SO₂ and NO_x emissions, which originate mainly from combustion processes, the uncertainty in NH₃ emissions is larger, being greater than $\pm 100\%$ (Kurokawa et al., 2013). Future studies should attempt to refine the emission inventory and understand the ef-

fect of emission uncertainties. The modeled total deposition of A was higher in India than in China. However, we cannot evaluate the model performance over India due to a lack of observation.

4.2 Ensemble approach

An ensemble approach was used with the aim of improving model performance. In MICS-Asia phase II, it was found that the model ensemble means better agreed with measurements of sulfate and total ammonium than the individual results from each model (Hayami et al., 2008). Other model comparison studies, such as the Air Quality Model Evaluation International Initiative (AQMEII) over north America and Europe, also noted better model performance through the ensemble mean (Solazzo et al., 2012). In MICS-Asia phase III, other companion papers also tried to use the ensemble approach for the gas species NO₂, NH₃, and CO (Kong et al., 2020), aerosols (Chen et al., 2019), and O₃ (Li et al., 2019). Here, we first used the following simple ensemble approach

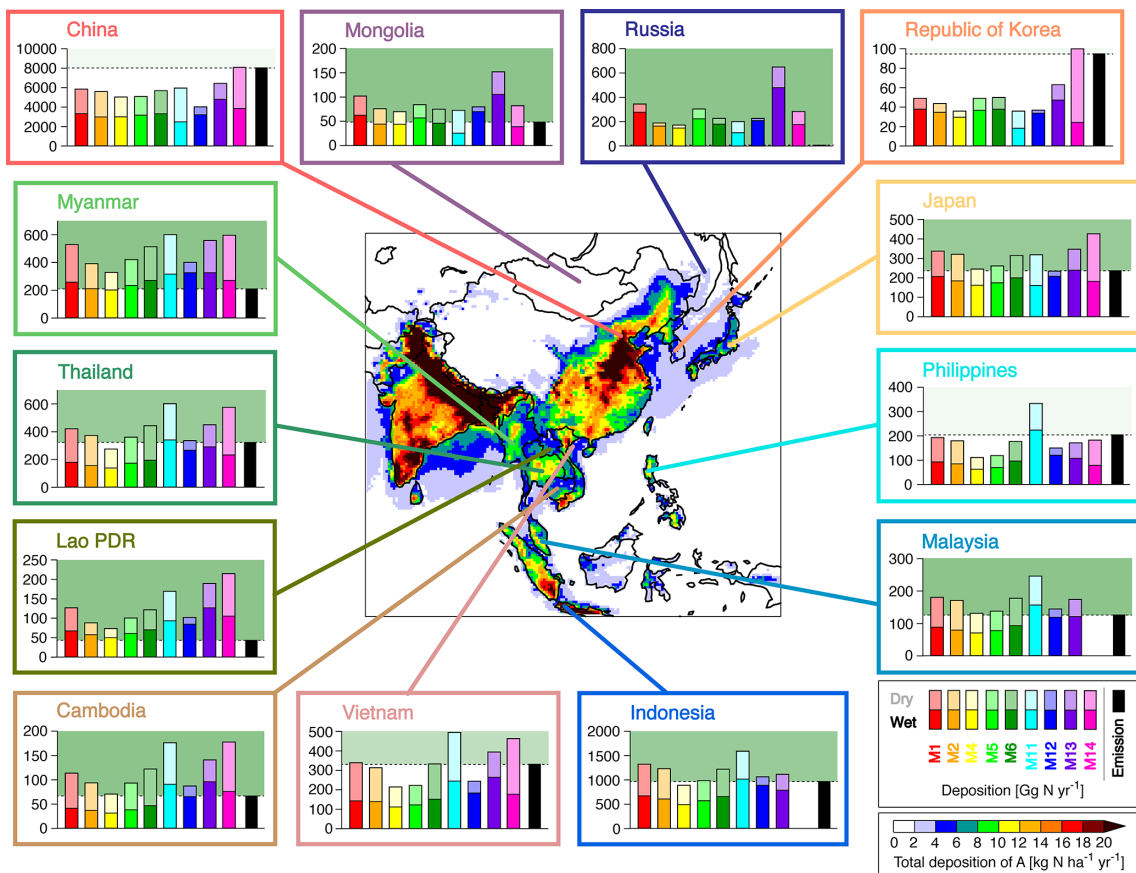


Figure 11. Map of the annual accumulated total A deposition over Asia. The cumulative bar graphs show dry deposition (light colors) and wet deposition (dark colors), with different colors representing different models and black representing the amount of anthropogenic NH₃ emissions. The background green areas of the graphs indicate the excess of total deposition compared to emissions, and their transparency is based on the number of models making this prediction (i.e., bolder colors indicate that more of the nine models simulated the excess).

with all models:

$$\text{ENS} = \frac{1}{N} \sum D, \quad (4)$$

where D is the deposition (i.e., dry, wet, and total deposition), ENS is the ensemble mean, and N is the number of models; usually, N is 9 but can be 7 or 8 in models M13 and M14 due to the different model domain used. ENS and its coefficient of variation (CV) were calculated, where CV is defined as the standard deviation divided by the mean; therefore, a large value of CV indicates inconsistency among models, while a small value indicates consistency among models. The ENS and CV of the wet deposition of S, N, and A are shown in Fig. 12, and those of the dry and total deposition of S, N, and A are, respectively, shown in Figs. S11 and S12. As shown in Fig. 12, the ENS for the wet deposition of S was high over China and Indonesia, that for the wet deposition of N was high over China, and that for the wet deposition of A was high over China, Indonesia, and India, as was also simulated by each model (Figs. 4, 6, and 8). It was clarified that the CV values corresponding to these areas of

high wet deposition were relatively small, with a similar result obtained in all models. These results were introduced in the performance for aerosol in MICS-Asia phase III (Chen et al., 2019) and phase II (Carmichael et al., 2008b). For example, over eastern China, where a remarkably large amount of wet deposition of S and A was simulated, CV values varied from approximately 0.1 to 0.3. Due to differences in model performance, a slightly higher value of CV, around 0.4, was reported for the wet deposition of N (see Sect. 3.2.2). Generally, CV values higher than 0.5 corresponded well to the area of small deposition amount, and CV values greater than 1.0 were found over Tibet, around Japan, and from eastern Vietnam to Taiwan for the wet deposition of S; over the southwestern boundary of the modeling domain for the wet deposition of N; and over the northwestern and southeastern boundaries of the modeling domain for the wet deposition of A.

Another ensemble mean approach to emphasize model performance is the weighted ensemble mean (WENS). In MICS-Asia phase II, the ratio of each R value to the sum was defined as the weighting factor (W) of the correspond-

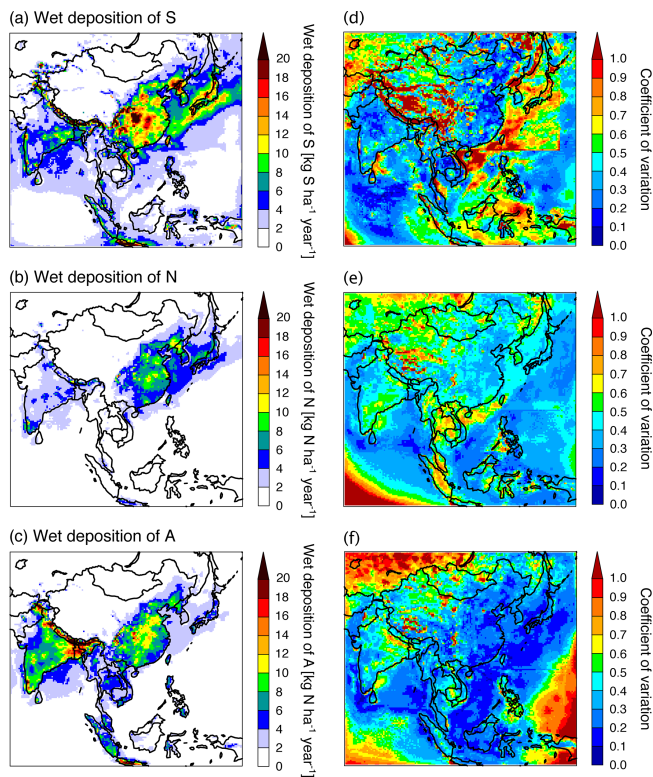


Figure 12. Spatial distributions of the ensemble mean (a–c) and the coefficient of variation (d–f) for the wet deposition of (a) S, (b) N, and (c) A.

ing model (Wang et al., 2008). Here, we also applied the R of model comparison results (Tables 3, 4, and 5) to derive the WENS as follows:

$$\text{WENS} = \frac{\sum(W \times D)}{\sum W}. \quad (5)$$

The results of the WENS are shown in Fig. 13. Overall, this approach gave results similar to those of ENS (shown in Fig. 12). The differences between ENS and WENS ($\text{ENS} - \text{WENS}$) were also calculated and are shown in Fig. 13. For the wet deposition of S, positive differences (i.e., higher values estimated by ENS than WENS) were found around some parts of eastern China, the Korean Peninsula, Japan and surrounding oceans, and eastern Vietnam to Taiwan. For these areas, models simulated high amounts of wet deposition, and there were large differences among models. Over these areas, models M11 and M12 simulated higher wet deposition than other models (see Fig. 4); however, values of R (i.e., weighting factors) were lower compared with other models (see Table 3). As a result, ENS led to higher wet deposition than WENS. Compared with the differences in the wet deposition of S between ENS and WENS, those of N and A were small; the differences were almost within $\pm 1.0 \text{ kg N ha}^{-1} \text{ yr}^{-1}$. This is because the values of R were similar among the models (see Tables 4 and 5), and almost

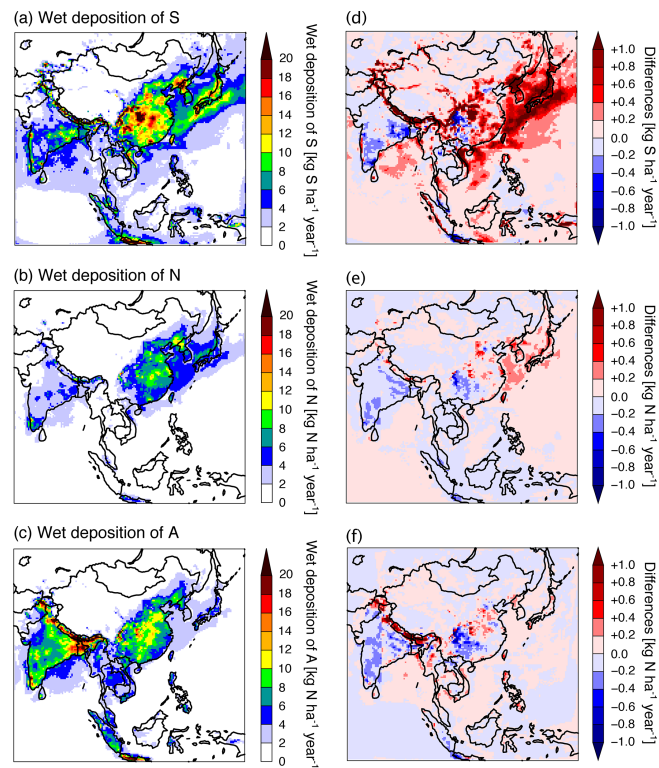


Figure 13. (a–c) Spatial distributions of the weighted ensemble mean for the wet deposition of (a) S, (b) N, and (c) A. (d–f) Differences between the ensemble mean and the weighted ensemble mean (calculated as ensemble mean – weighted ensemble mean).

the same estimation was obtained with ENS and WENS, even though there were large differences in the amount of wet deposition.

The statistical performance obtained by ENS and WENS is listed in Tables 6 to 8. For the wet deposition of S (Table 6), since only model M11 produced overestimation, ENS showed a negative NMB, and the R values of model M11 were lower compared with those of other models. WENS showed a larger NMB. In terms of NME, FAC2, and FAC3, ENS and WENS produced comparable results to those of model M13, which performed the best regarding NME, FAC2, and FAC3. For the wet deposition of N (Table 7), each model performed differently, and both ENS and WENS performed well in canceling the large outlier of each model performance. For the wet deposition of A (Table 8), ENS and WENS also performed well in canceling the large outlier of each model performance, as was observed for the wet deposition of N. In terms of NME, model M14 performed best, and ENS, and especially WENS, showed comparable results. In summary, the ensemble and weighted ensemble approaches were confirmed to be better ways to improve the model performance, allowing the elimination of extreme performance. In terms of NMB, ENS performed better than WENS; however, WENS could be regarded as a better approach because

it takes into account each model performance evaluated by observation using R as the weighting factor and it showed better values than ENS in terms of NME, FAC2, and FAC3.

4.3 Precipitation-adjusted approach

In Sect. 4.2, it was confirmed that the ensemble approach and the weighted ensemble approach, which considered R as a weighting factor, improved model performance for wet deposition and were effective at modulating the differences between models. Here, we sought a way to improve model performance and focused on the reproducibility of precipitation. The model performance for precipitation is clearly an important factor for wet deposition. In MICS-Asia phase III, the meteorological field was basically coordinated in WRF, and three types of meteorological models were used (WRF, GEOS-5, and RAMS). Although the precipitation performance of all of the models generally captured the observed precipitation, their behavior was different – for example, WRF and GEOS-5 slightly overestimated and RAMS underestimated the precipitation, as discussed in Sect. 3.1. It is interesting that, compared with EANET observations, the model performance for the wet deposition of S, N, and A was found to have remarkably higher R values for models M13 and M14 driven by the different models of GEOS-5 and RAMS. Such model performance for wet deposition might be partly due to the differences in precipitation. The precipitation-adjusted approach linearly scaled the precipitation amount to obtain the precipitation-adjusted wet deposition by the following equation:

$$\text{Adjusted WD} = \sum_{\text{monthly}} \text{Original WD}_{\text{model}} \times \frac{\sum_{\text{monthly}} P_{\text{observation}}}{\sum_{\text{monthly}} P_{\text{model}}}, \quad (6)$$

where WD_{model} is the original modeled wet deposition and P_{model} and $P_{\text{observation}}$ are the modeled and observed precipitation amounts, respectively. This approach has been used in previous studies over the US (Appel et al., 2011; Zhang et al., 2018) and Asia (Itahashi, 2018). Note that this precipitation-adjusted approach assumes that errors associated with the modeled precipitation are linearly related to errors in wet deposition amounts and the precipitation was adjusted by the total amount of observed precipitation; hence, the modeled convective and subgrid-scale precipitation was not distinguished. Because current meteorological models have difficulty in capturing the timing of precipitation events, the application of this adjusted approach at a finer temporal resolution will lead to excessive adjustments (e.g., close to zero in the case that observed precipitation is zero or divergent in the case that the modeled precipitation is near zero). Therefore, in this study, wet deposition was adjusted for precipitation on a monthly timescale, and then the annual precipitation-adjusted wet deposition was calculated. To verify this ap-

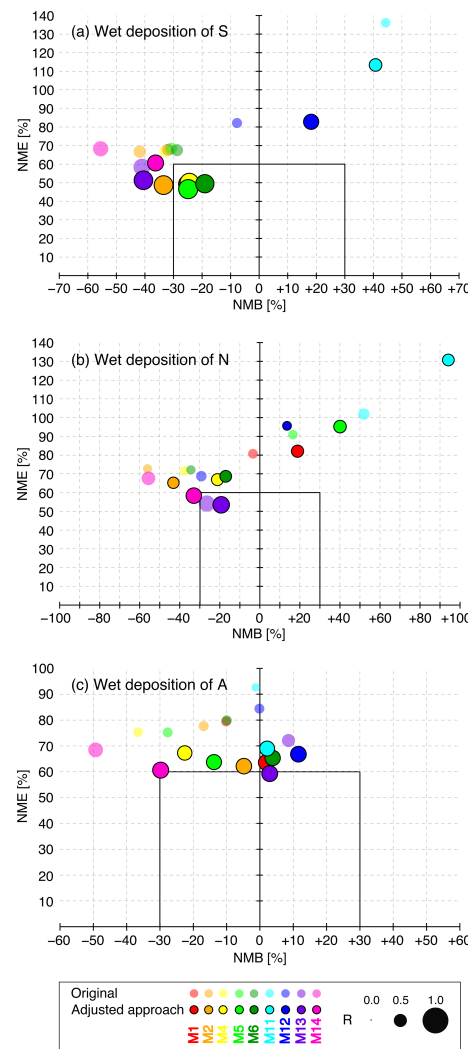


Figure 14. Soccer-goal plot of NMB (x axis) and NME (y axis) for the original wet deposition (transparent circles) and precipitation-adjusted wet deposition (solid circles) of (a) S, (b) N, and (c) A. The size of each circle indicates R . Note that the ranges of NMB and NME are different among the three panels.

proach, soccer-goal plots in terms of NMB and NME were created for the wet deposition of S, N, and A, as shown in Fig. 14. In these plots, R is indicated by the size of the circle.

For the wet deposition of S (Fig. 14a), the improvement of model performance was clear; all of the model results were close to the soccer goal, and the size of the circle was larger. The model performance for the wet deposition of S improved values of R to above 0.7 for models M1, M2, M4, M5, and M6, above 0.5 for model M11, and above 0.6 for model M12; all of these models were driven by the WRF meteorological model. For model M13, which was driven by the GEOS-5 model, an R value of 0.74 was obtained, and an R value of 0.64 was obtained for model M14, which was driven by the RAMS model. The underestimation, as shown

Table 6. Summary of statistical analysis of model performance by the ensemble and precipitation-adjusted approaches for the wet deposition of S.

Model	Ensemble mean	Weighted ensemble mean	Ensemble mean of precipitation-adjusted wet deposition	Weighted ensemble mean of precipitation-adjusted wet deposition
<i>N</i>		588		
Mean (observation) ($\text{g S ha}^{-1} \text{ month}^{-1}$)		876.5		
Mean (model) ($\text{g S ha}^{-1} \text{ month}^{-1}$)	675.4	615.9	739.4	649.5
<i>R</i>	0.47	0.51	0.76	0.76
NMB (%)	-22.9	-29.7	-15.6	-19.9
NME (%)	+66.5	+62.8	+48.4	+47.1
FAC2 (%)	45.1	45.9	62.9	62.9
FAC3 (%)	63.1	63.8	81.6	81.8

Table 7. Summary of the statistical analysis of model performance by ensemble and precipitation-adjusted approaches for the wet deposition of N.

Model	Ensemble mean	Weighted ensemble mean	Ensemble mean of precipitation-adjusted wet deposition	Weighted ensemble mean of precipitation-adjusted wet deposition
<i>N</i>		575		
Mean (observation) ($\text{g N ha}^{-1} \text{ month}^{-1}$)		347.5		
Mean (model) ($\text{g N ha}^{-1} \text{ month}^{-1}$)	282.6	271.2	359.0	347.1
<i>R</i>	0.43	0.44	0.52	0.53
NMB (%)	-19.1	-22.4	+3.2	-0.3
NME (%)	+67.2	+65.0	+68.3	+66.4
FAC2 (%)	46.8	47.5	52.9	53.6
FAC3 (%)	66.3	68.0	74.8	73.9

Table 8. Summary of the statistical analysis of model performance by ensemble and precipitation-adjusted approaches for the wet deposition of A.

Model	Ensemble mean	Weighted ensemble mean	Ensemble mean of precipitation-adjusted wet deposition	Weighted ensemble mean of precipitation-adjusted wet deposition
<i>N</i>		568		
Mean (observation) ($\text{g N ha}^{-1} \text{ month}^{-1}$)		440.7		
Mean (model) ($\text{g N ha}^{-1} \text{ month}^{-1}$)	378.3	358.5	420.2	411.8
<i>R</i>	0.41	0.45	0.66	0.66
NMB (%)	-13.6	-18.4	-4.6	-6.6
NME (%)	+74.6	+70.8	+58.0	+57.6
FAC2 (%)	38.0	41.4	57.4	57.6
FAC3 (%)	59.5	61.4	76.4	76.9

by negative NMB, was improved by 10 %–20 %, and NME was also improved by 10 %–20 % for models M1, M2, M4, M5, M6, M13, and M14. The overestimation for model M11, as shown by positive NMB, was improved by 5 %, and NME was improved by more than 20 %. For model M12, NMB changed sign from negative bias to positive bias and NME was almost unchanged. We further conducted the ensemble approach for this precipitation-adjusted wet deposition. The statistical analysis is listed in Table 6. The ENS based on

the precipitation-adjusted wet deposition showed an *R* value of 0.76, and both NMB and NME were improved compared with ENS based on the original wet deposition, also showing a better correspondence with observation; over 60 % were within FAC2 and over 80 % were within FAC3. The WENS based on the precipitation-adjusted approach also performed reasonably well and achieved a slightly worse NMB score, but other scores were almost the same for the ENS based on the precipitation-adjusted wet deposition.

For the wet deposition of N (Fig. 14b), the results from the precipitation-adjusted approach were complicated. CMAQ models M1, M2, M4, M5, and M6, which were driven by WRF, showed an improvement of R ; however, the values were different, ranging from 0.58 for M5 to 0.74 for M4. Since the wet deposition of N was differently calculated, even in CMAQ models, this precipitation-adjusted approach led to a better NMB for models M2, M4, and M6, whereas it led to a worse NMB for models M1 and M5; however, the latter two models showed almost no change in NME. Models M11 and M12, which were driven by WRF, did not show improvement in R through the precipitation-adjusted approach; the values of R were slightly reduced, and those of NME were reduced by more than 20 %. The difference in performance between the original and precipitation-adjusted wet deposition was not dramatic for model M13, which was driven by GEOS-5, and it revealed improvement for model M14, which was driven by RAMS, in terms of R , NMB, and NME. Thus, the use of ENS and WENS for the precipitation-adjusted approach listed in Table 7 achieves better performance for R and NMB but no improvement in NME. Additionally, the corresponding percentages were improved.

For the wet deposition of A (Fig. 14c), the precipitation-adjusted approach clearly improved the model performance. All model soccer-goal plots were close to the center of the goal, and the sizes of the plots were enlarged; all models obtained R values of around 0.6. Generally, both NMB and NME were improved by about 10 %, but model M12 changed to a slight overestimation. For model M13, which was driven by GEOS-5, a reduction of overestimation was found. Therefore, the statistical performance of ENS and WENS, as listed in Table 8, suggests improvements of the original wet deposition simulations.

With the use of the precipitation-adjusted approach, overall improvements in model performance were shown, regardless of the original meteorological field. This result suggests the importance of the accuracy of modeled precipitation for the modeling of wet deposition. However, the precipitation-adjusted approach was not effective in terms of NME for the wet deposition of N. The mechanism of the wet deposition process should be further investigated in future research.

5 Concluding remarks and future perspectives for phase IV

MICS-Asia phase III was conducted in order to understand the current modeling capabilities in Asia. In this overview of deposition, simulations of deposition by nine models were analyzed. The modeled wet deposition of S, N, and A was evaluated by comparison with the wet deposition observed by EANET. Generally, the models can capture the observed wet deposition, albeit with underestimation for S and A and large variability among models for N. Comparisons of atmospheric concentrations revealed that model performance is

either characterized by an inverse relationship between the overestimation (underestimation) of the wet deposition of S and the underestimation (overestimation) of the atmospheric concentration of S or characterized by the underestimation of both the atmospheric concentration and wet deposition of S species. It was clarified as an inverse relationship on the underestimation of wet deposition of A and the overestimation of atmospheric concentration of A. The relationships between atmospheric concentration and wet deposition of N are complicated, and further research focusing on nitrogen species especially targeting the nitrogen cycle is required. Then, we moved to a discussion of the importance of dry and wet deposition to total deposition and presented maps of the total deposition over Asia. The balance between deposition and emissions was analyzed and revealed the possibility of a contribution from long-range transport. We also discussed ways to improve modeling results by taking an ensemble approach and a weighted ensemble approach using R as a weighting factor, and by using a precipitation-adjusted approach. Both approaches can successfully be applied to improve model performance.

In this overview paper, a model evaluation was conducted by comparison with EANET observations. Over China, which showed the highest amount of deposition over Asia, EANET data were available at eight sites in four regions. The available observations in China have been limited over the past decades; however, there are extensive observations to capture them. A detailed model intercomparison over China based on the available observations will be reported in work following our companion paper (Ge et al., 2020). Additionally, we limited the evaluation to wet deposition, due to the difficulty of measuring dry deposition, and relied on the model performance to determine atmospheric concentrations. In the EANET framework, an inferential method was used that utilizes multiple observed atmospheric concentrations and estimated dry deposition velocities. A detailed discussion of modeled dry deposition comparing the inferential method will be presented in our forthcoming companion research.

To further understand S, investigating the behavior of Na^+ as a sea-salt (ss) tracer would be valuable to separately analyze ss and non-ss (nss) SO_4^{2-} concentration and deposition. This is especially important in coastal areas. In the phase III study, large discrepancies were found over Japan for the wet deposition of S. This point should be considered in phase IV. Moreover, the balance among S, N, and A should be further studied. Along with the drastic changes of emissions in China (Li et al., 2017b), it has been demonstrated that the key species in terms of acid deposition over east Asia has changed from S to N (Itahashi et al., 2014, 2015, 2018a). In the phase III study, we conducted a full-year model simulation for 2010 and were able to estimate the annual accumulated deposition over Asia from multi-model intercomparison for the first time. On the one hand, it is further necessary to conduct longer-term intercomparison, since the meteorol-

ogy (i.e., precipitation) has year-to-year variation and it is not known how large variations result from the multi-model intercomparisons. One example is that wet deposition over the Republic of Korea was higher than that over Japan in 2010 but this tendency was reversed in other years (EANET, 2016a, b). On the other hand, it is also necessary to focus on case studies, such as severe rainfall events. Although we can provide an overview of the modeled deposition for annual accumulation from phase III, we did not conduct a detailed analysis of model performance, especially in terms of temporal variation (e.g., intense rain events). The use of different temporal coverages would be a potentially useful approach in phase IV. Moreover, precipitation type (convective or non-convective) should be analyzed, and the impacts of differences in the characteristics of fine and coarse particles on wet deposition should be investigated. The updating of emissions from 2010 will also be required to account for the recent drastic changes over China and southeast Asian countries.

Finally, adjustment for precipitation in phase III revealed a potential way to improve the simulation of wet deposition. The model performance for precipitation and related parameters (e.g., water vapor mixing ratio) should be refined in phase IV as the key input data to CTMs. This approach could constitute one of the methodologies in the Measurement–Model Fusion for Global Total Atmospheric Deposition (MMF-GTAD) project under the Global Atmosphere Watch (GAW) program of the World Meteorological Organization (WMO) (World Meteorological Organization Global Atmosphere Watch, 2017).

Data availability. The EANET observational dataset used in this study is available at <http://www.eanet.asia> (EANET, 2019a) (last access: 1 November 2019).

Supplement. The supplement related to this article is available online at: <https://doi.org/10.5194/acp-20-2667-2020-supplement>.

Author contributions. SI led the deposition analysis group in MICS-Asia III, performed one of the model simulations, and prepared the manuscript with contributions from all co-authors. BG and KS are the members of the deposition analysis group in MICS-Asia III and discussed the results with SI. JSF, XW, KY, TN, JL, BG, MK, HL, and MZ performed the model simulations and contributed by submitting their simulated deposition results. ZW performed the meteorological model simulation and examined the model performance. ML and JK prepared the emission inventory data. MICS-Asia III was coordinated by GRC and ZW.

Competing interests. The authors declare that they have no conflict of interest.

Special issue statement. This article is part of the special issue ‘Regional assessment of air pollution and climate change over East and Southeast Asia: results from MICS-Asia Phase III’. It is not associated with a conference.

Acknowledgements. The authors thank EANET for providing wet deposition measurement data over Asia. The authors are grateful to Kengo Sudo from Nagoya University, Japan, and Rokjin J. Park from Seoul National University, South Korea, for providing us with the CHASER and GEOS-Chem data as the lateral boundary condition. This work was partly supported by the Global Environment Research Fund (no. S-12) of the Ministry of the Environment, Japan. This work was also supported by JSPS KAKENHI (grant no. JP16K21690). Part of this work was also funded by the National Natural Science Foundation of China (grant no. 41620104008). This work was also supported by Chinese National Key Research and Development Plan (20017YFC0210105).

Financial support. This research has been supported by the Global Environment Research Fund (no. S-12) of the Ministry of the Environment, Japan and JSPS KAKENHI (grant no. JP16K21690).

Review statement. This paper was edited by Andrea Pozzer and reviewed by two anonymous referees.

References

- Aerosol Comparison between Observations and Models (AERO-COM): Emission data download, available at: https://aerocom.met.no/DATA/download/emissions/AEROCOM_HC/volc/, last access: 12 March 2019.
- Akimoto, H., Nagashima, T., Li, J., Fu, J. S., Ji, D., Tan, J., and Wang, Z.: Comparison of surface ozone simulation among selected regional models in MICS-Asia III – effects of chemistry and vertical transport for the causes of difference, *Atmos. Chem. Phys.*, 19, 603–615, <https://doi.org/10.5194/acp-19-603-2019>, 2019.
- Appel, K. W., Foley, K. M., Bash, J. O., Pinder, R. W., Dennis, R. L., Allen, D. J., and Pickering, K.: A multi-resolution assessment of the Community Multiscale Air Quality (CMAQ) model v4.7 wet deposition estimates for 2002–2006, *Geosci. Model Dev.*, 4, 357–371, <https://doi.org/10.5194/gmd-4-357-2011>, 2011.
- Bey, I., Jacob, D. J., Yantosca, R. M., Logan, J. A., Field, B., Fiore, A. M., Li, Q., Liu, H., Mickley, L. J., and Schultz, M.: Global modeling of tropospheric chemistry with assimilated meteorology: model description and evaluation, *J. Geophys. Res.*, 106, 23073–23095, 2001.
- Bleeker, A., Hicks, W. K., Dentener, F., Galloway, J., and Erisman, J. W.: N deposition as a threat to the world’s protected areas under the convention on biological diversity, *Environ. Pollut.*, 159, 2280–2288, <https://doi.org/10.1016/j.envpol.2010.10.036>, 2011.
- Byun, D. W. and Dennis, R. L.: Design artifacts in Eulerian air quality models: Evaluation of the effects of layer thickness and vertical profile correction on surface ozone concentrations, *Atmos. Environ.*, 29, 105–126, 1995.

- Byun, D. and Schere, K. L.: Review of the governing equations, computational algorithms, and other components of the models-3 Community Multiscale Air Quality (CMAQ) modeling system, *Appl. Mech. Rev.*, 59, 51–77, <https://doi.org/10.1115/1.2128636>, 2006.
- Carlton, A. G., Bhave, P. V., Napelenok, S. L., Edney, E. O., Sarwar, G., Pinder, R. W., Pouliot, G. A., and Houyoux, M.: Model representation of secondary organic aerosol in CMAQv4.7, *Environ. Sci. Technol.*, 44, 8553–8560, <https://doi.org/10.1021/es100636q>, 2010.
- Carmichael, G. R., Calori, G., Hayami, H., Uno, I., Cho, S. Y., Engardt, M., Kim, S.-B., Ichikawa, Y., Ikeda, Y., Woo, J.-H., Ueda, H., and Amann, M., The MICS-Asia study: model intercomparison of long-range transport and sulfur deposition in East Asia, *Atmos. Environ.*, 36, 175–199, 2002.
- Carmichael, G. R., Sandu, A., Chai, T., Daescu, D. N., Constantinescu, E. M., and Tang, Y.: Predicting air quality: Improvements through advanced methods to integrate models and measurements, *J. Comp. Phys.*, 227, 3540–3571, <https://doi.org/10.1016/j.jcp.2007.02.024>, 2008a.
- Carmichael, G. R., Sakurai, T., Streets, D., Hozumi, Y., Ueda, H., Park, S. U., Fung, C., Han, Z., Kajino, M., Engardt, M., Bennet, C., Hayami, H., Sartelet, K., Holloway, T., Wang, Z., Kannari, A., Fu, J., Matsuda, K., Thongboonchoo, N., and Amann, M., MICS-Asia II: The model intercomparison study for Asia Phase II methodology and overview of findings, *Atmos. Environ.*, 42, 3468–3490, 2008b.
- Carter, W. L.: Implementation of the SAPRC-99 chemical mechanism into the Models-3 framework, Report to the United States Environmental Protection Agency, available at: <https://intra.cert.ucr.edu/~carter/pubs/s99mod3.pdf> (last access: 14 February 2020), 2000.
- Chang, J. S., Brost, R. A., Isaksen, S. A., Madronich, S., Middleton, P., Stockwell, W. R., and Walcek, C. J.: A three-dimensional eulerian acid deposition model: Physical concepts and formulation, *J. Geophys. Res.*, 92, 14681–14700, 1987.
- Chen, F., Kusaka, H., Bornstain, R., Ching, J., Grimmond, C. S. B., Grossman-Clarke, S., Loridan, T., Manning, K., Martilli, A., Miao, S., Sailor, D., Salamanca, F., Taha, H., Tewari, M., Wang, X., Wyszogrodzki, A., and Zhang, C.: The integrated WRF/urban modeling system: development, evaluation, and applications to urban environmental problems, *Int. J. Climatol.*, 31, 273–288, <https://doi.org/10.1002/joc.2158>, 2011.
- Chen, L., Gao, Y., Zhang, M., Fu, J. S., Zhu, J., Liao, H., Li, J., Huang, K., Ge, B., Wang, X., Lam, Y. F., Lin, C.-Y., Itahashi, S., Nagashima, T., Kajino, M., Yamaji, K., Wang, Z., and Kurokawa, J.: MICS-Asia III: multi-model comparison and evaluation of aerosol over East Asia, *Atmos. Chem. Phys.*, 19, 11911–11937, <https://doi.org/10.5194/acp-19-11911-2019>, 2019.
- Chen, S.-H. and Sun, W.-Y.: A one-dimensional time dependent cloud model, *J. Meteorol. Soc. Jpn.*, 80, 99–118, 2002.
- Chou, M.-D. and Suarez, M. J.: An efficient thermal infrared radiation parameterization for use in general circulation models, NASA Tech. Memo. 104606, 3, 85 pp., 1994.
- Clean Air Status and Trends Networks (CASTNET): <https://www.epa.gov/castnet>, last access: 25 February 2019.
- Colella, P. and Woodward, P. R.: The piecewise parabolic method (PPM) for gas dynamical simulations, *J. Comp. Phys.*, 54, 174–201, 1984.
- EANET: Quality assurance/quality control (QA/QC) program for wet deposition monitoring in East Asia, available at: <https://www.eanet.asia/wp-content/uploads/2019/04/qaqcwet.pdf> (last access: 14 February 2020), 2000.
- EANET: Technical manual for wet deposition monitoring in East Asia, available at: <https://www.eanet.asia/wp-content/uploads/2019/04/techwet.pdf> (last access: 14 February 2020), 2010a.
- EANET: Technical manual on dry deposition flux estimation in East Asia, available at: <https://www.eanet.asia/wp-content/uploads/2019/04/techdry.pdf> (last access: 14 February 2020), 2010b.
- EANET: Periodic report on the state of acid deposition in East Asia, Part I: Regional assessment. Acid Deposition Monitoring Network in East Asia, available at: https://www.eanet.asia/wp-content/uploads/2019/04/1_PRSAD1-1.pdf (last access: 14 February 2020), 2006a.
- EANET: Periodic report on the state of acid deposition in East Asia, Part II: National assessments, Acid Deposition Monitoring Network in East Asia, available at: https://www.eanet.asia/wp-content/uploads/2019/04/1_PRSAD2-1.pdf (last access: 14 February 2020), 2006b.
- EANET: Second periodic report on the state of acid deposition in East Asia, Part I: Regional assessment, Acid Deposition Monitoring Network in East Asia, available at: http://www.eanet.asia/wp-content/uploads/2019/03/2_PRSAD1.pdf (last access: 14 February 2020), 2011a.
- EANET: Second periodic report on the state of acid deposition in East Asia, Part II: National assessments, Acid Deposition Monitoring Network in East Asia, available at: https://www.eanet.asia/wp-content/uploads/2019/04/2_PRSAD2.pdf (last access: 14 February 2020), 2011b.
- EANET: Review on the state of air pollution in East Asia. Task Force on Research Coordination, Scientific Advisory Committee, Acid Deposition Monitoring Network in East Asia, available at: <https://www.eanet.asia/wp-content/uploads/2019/04/RSAP.pdf> (last access: 14 February 2020), 2015.
- EANET: Third periodic report on the state of acid deposition in East Asia, Part I: Regional assessment, Acid Deposition Monitoring Network in East Asia, available at: https://www.eanet.asia/wp-content/uploads/2019/03/3_PRSAD1.pdf (last access: 14 February 2020), 2016a.
- EANET: Third periodic report on the state of acid deposition in East Asia, Part II: National assessments, Acid Deposition Monitoring Network in East Asia, available at: https://www.eanet.asia/wp-content/uploads/2019/03/3_PRSAD2.pdf (last access: 14 February 2020), 2016b.
- EANET: available at: <http://www.eanet.asia>, last access: 1 November 2019a.
- EANET: Data Report, available at: <https://monitoring.eanet.asia/document/public/index>, last access: 1 November 2019b.
- European Monitoring and Evaluation Programme (EMEP): <https://www.emep.int>, last access: 25 February 2019.
- Foley, K. M., Roselle, S. J., Appel, K. W., Bhave, P. V., Pleim, J. E., Otte, T. L., Mathur, R., Sarwar, G., Young, J. O., Gilliam, R. C., Nolte, C. G., Kelly, J. T., Gilliland, A. B., and Bash, J. O.: Incremental testing of the Community Multiscale Air Quality (CMAQ) modeling system version 4.7, *Geosci. Model Dev.*, 3, 205–226, <https://doi.org/10.5194/gmd-3-205-2010>, 2010.
- Fountoukis, C. and Nenes, A.: ISORROPIA II: a computationally efficient thermodynamic equilibrium model for K⁺–

- Ca^{2+} – Mg^{2+} – NH_4^+ – Na^+ – SO_4^{2-} – NO_3^- – Cl^- – H_2O aerosols, *Atmos. Chem. Phys.*, 7, 4639–4659, <https://doi.org/10.5194/acp-7-4639-2007>, 2007.
- Fujita, S., Takahashi, A., Weng, J.-H., Huang, L.-F., Kim, H.-K., Li, C.-K., Huang, F. T. C., and Jeng, F.-T.: Precipitation chemistry in East Asia, *Atmos. Environ.*, 34, 525–537, 2000.
- Gao, M., Han, Z., Liu, Z., Li, M., Xin, J., Tao, Z., Li, J., Kang, J.-E., Huang, K., Dong, X., Zhuang, B., Li, S., Ge, B., Wu, Q., Cheng, Y., Wang, Y., Lee, H.-J., Kim, C.-H., Fu, J. S., Wang, T., Chin, M., Woo, J.-H., Zhang, Q., Wang, Z., and Carmichael, G. R.: Air quality and climate change, Topic 3 of the Model Inter-Comparison Study for Asia Phase III (MICS-Asia III) – Part 1: Overview and model evaluation, *Atmos. Chem. Phys.*, 18, 4859–4884, <https://doi.org/10.5194/acp-18-4859-2018>, 2018.
- Ge, B. Z., Wang, Z. F., Xu, X. B., Wu, J. B., Yu, X. L., and Li, J.: Wet deposition of acidifying substances in different regions of China and the rest of East Asia: Modeling with updated NAQPMs, *Environ. Pollut.*, 187, 10–21, 2014.
- Ge, B., Itahashi, S., Sato, K., Xu, D., Wang, J., Fan, F., Tan, Q., Fu, J. S., Wang, X., Yamaji, K., Nagashima, T., Li, J., Kajino, M., Liao, H., Zhang, M., Wang, Z., Li, M., Woo, J.-H., Kurokawa, J., Pan, Y., Wu, Q., Liu, X., and Wang, Z.: MICS-Asia III: Multi-model comparison of reactive Nitrogen deposition over China, *Atmos. Chem. Phys. Discuss.*, <https://doi.org/10.5194/acp-2019-1083>, in review, 2020.
- Grell, G. A.: Prognostic Evaluation of Assumptions Used by Cumulus Parameterizations, *Mon. Weather Rev.*, 121, 764–787, 1993.
- Grell, G. A. and Devenyi, D.: A generalized approach to parameterizing convection combining ensemble and data assimilation techniques, *Geophys. Res. Lett.*, 29, 1693, <https://doi.org/10.1029/2002GL015311>, 2002.
- Guenther, A., Karl, T., Harley, P., Wiedinmyer, C., Palmer, P. I., and Geron, C.: Estimates of global terrestrial isoprene emissions using MEGAN (Model of Emissions of Gases and Aerosols from Nature), *Atmos. Chem. Phys.*, 6, 3181–3210, <https://doi.org/10.5194/acp-6-3181-2006>, 2006.
- Hayami, H., Sakurai, T., Han, Z., Ueda, H., Carmichael, G. R., Streets, D., Holloway, T., Wang, Z., Thongboonchoo, N., Engardt, M., Bennet, C., Fung, C., Chang, A., Park, S. U., Sartelet, K., Matsuda, K., and Amann, M.: MICS-Asia II: Model inter-comparison and evaluation of particulate sulfate, nitrate and ammonium, *Atmos. Environ.*, 42, 3510–3527, 2008.
- Holtslag, A. A. M. and Boville, B.: Local versus nonlocal boundary layer diffusion in a global climate model, *J. Climate*, 6, 1825–1842, 1993.
- Hong, S.-Y., Noh, Y., and Dudhia, J.: A new vertical diffusion package with an explicit treatment of entrainment processes, *Mon. Weather Rev.*, 134, 2318–2341, 2006.
- Huang, X., Song, Y., Li, M., Li, J., Huo, Q., Cai, X., Zhu, T., Hu, M., and Zhang, H.: A high-resolution ammonia emission inventory in China, *Global Biogeochem. Cy.*, 26, GB1030, <https://doi.org/10.1029/2011GB004161>, 2012.
- Itahashi, S.: Toward synchronous evaluation of source apportionments for atmospheric concentration and deposition of sulfate aerosol over East Asia, *J. Geophys. Res.*, 123, 2927–2953, 2018.
- Itahashi, S., Uno, I., Hayami, H., and Fujita, S.: Modeling investigation of controlling factors in the increasing ratio of nitrate to non-seasalt sulfate in precipitation over Japan, *Atmos. Environ.*, 92, 171–177, <https://doi.org/10.1016/j.atmosenv.2014.04.022>, 2014.
- Itahashi, S., Uno, I., Hayami, H., and Fujita, S.: Variation of the ratio of nitrate to non-seasalt sulfate in precipitation over East Asia with emissions from China, *Atmos. Environ.*, 118, 87–97, <https://doi.org/10.1016/j.atmosenv.2015.07.032>, 2015.
- Itahashi, S., Hayami, H., Uno, I., Pan, X., and Uematsu, M.: Importance of coarse-mode nitrate produced via sea-salt as atmospheric input to East Asian oceans, *Geophys. Res. Lett.*, 43, 5483–5491, <https://doi.org/10.1002/2016GL068722>, 2016.
- Itahashi, S., Hayami, H., Yumimoto, K., and Uno, I.: Chinese province-scale source apportionments for sulfate aerosol in 2005 evaluated by the tagged tracer method, *Environ. Pollut.*, 220, 1366–1375, 2017.
- Itahashi, S., Yumimoto, K., Uno, I., Hayami, H., Fujita, S.-I., Pan, Y., and Wang, Y.: A 15-year record (2001–2015) of the ratio of nitrate to non-sea-salt sulfate in precipitation over East Asia, *Atmos. Chem. Phys.*, 18, 2835–2852, <https://doi.org/10.5194/acp-18-2835-2018>, 2018a.
- Itahashi, S., Yamaji, K., Chatani, S., and Hayami, H.: Refinement of modeled aqueous-phase sulfate production via the Fe- and Mn-catalyzed oxidation pathway, *Atmosphere*, 9, 132, <https://doi.org/10.3390/atmos9040132>, 2018b.
- Itahashi, S., Yamaji, K., Chatani, S., Hisatsune, K., Saito, S., and Hayami, H.: Model performance differences in sulfate aerosol in winter over Japan based on regional chemical transport models of CMAQ and CAMx, *Atmosphere*, 9, 488, <https://doi.org/10.3390/atmos9120488>, 2018c.
- Itahashi, S., Yamaji, K., Chatani, S., and Hayami, H.: Differences in model performance and source sensitivities for sulfate aerosol resulting from updates of the aqueous- and gas-phase oxidation pathways for a winter pollution episode in Tokyo, Japan, *Atmosphere*, 10, 544, <https://doi.org/10.3390/atmos10090544>, 2019.
- Janjic, Z.: The step-mountain eta coordinate model: Further developments of the convection, viscous sublayer, and turbulence closure schemes, *Mon. Weather Rev.*, 122, 927–945, 1994.
- Jiménez, P. A., Dudhia, J., Gonzalez-Rouco, J. F., Navarro, J., Montavez, J. P., and Garcia-Bustamante, E.: A revised scheme for the WRF surface layer formulation, *Mon. Weather Rev.*, 140, 898–918, <https://doi.org/10.1175/MWR-D-11-00056.1>, 2012.
- JPEC (Japan Petroleum Energy Center): Emission inventory of road transport in Japan, JPEC, Tokyo, Japan, JPEC Technical Report, JPEC-2011AQ-02-06, 136 pp., 2012a (in Japanese).
- JPEC: Emission inventory of sources other than road transport in Japan, JPEC, Tokyo, Japan, JPEC Technical Report, JPEC-2011AQ-02-07, 288 pp., 2012b (in Japanese).
- JPEC: Speciation profiles of VOC, PM, and NO_x emissions for atmospheric simulations of $\text{PM}_{2.5}$, JPEC, Tokyo, Japan, JPEC Technical Report, JPEC-2011AQ-02-08, 69 pp., 2012c (in Japanese).
- Kajino, M., Ueda, H., Sato, K., and Sakurai, T.: Spatial distribution of the source-receptor relationship of sulfur in Northeast Asia, *Atmos. Chem. Phys.*, 11, 6475–6491, <https://doi.org/10.5194/acp-11-6475-2011>, 2011.
- Kajino, M., Sato, K., Inomata, Y., and Ueda, H.: Source-receptor relationships of nitrate in Northeast Asia and influence of sea salt on the long-range transport of nitrate, *Atmos. Environ.*, 59, 461–475, <https://doi.org/10.1016/j.atmosenv.2013.06.024>, 2013.
- Kajino, M., Deushi, M., Sekiyama, T. T., Oshima, N., Yumimoto, K., Tanaka, T. Y., Ching, J., Hashimoto, A., Yamamoto, T., Ikegami, M., Kamada, A., Miyashita, M., Inomata, Y., Shima,

- S., Adachi, K., Zaizen, Y., Igarashi, Y., Ueda, H., Maki, T., and Mikami, M.: NHM-Chem, the Japan Meteorological Agency's regional meteorology – chemistry model (v1.0): model description and aerosol representations, *Geosci. Model Dev. Discuss.*, <https://doi.org/10.5194/gmd-2018-128>, 2018.
- Kajino, M., Deushi, M., Sekiyama, T. T., Oshima, N., Yumimoto, K., Tanaka, T. Y., Ching, J., Hashimoto, A., Yamamoto, T., Ikegami, M., Kamada, A., Miyashita, M., Inomata, Y., Shima, S., Takami, A., Shimizu, A., Hatakeyama, S., Sadanaga, Y., Irie, H., Adachi, K., Zaizen, Y., Igarashi, Y., Ueda, H., Maki, T., and Mikami, M.: NHM-Chem, the Japan Meteorological Agency's regional meteorology – chemistry model: model evaluations toward the consistent predictions of the chemical, physical and optical properties of aerosols, *J. Meteorol. Soc. Jpn.*, 97, 337–374, <https://doi.org/10.2151/jmsj.2019-020>, 2019.
- Kong, L., Tang, X., Zhu, J., Wang, Z., Fu, J. S., Wang, X., Itahashi, S., Yamaji, K., Nagashima, T., Lee, H.-J., Kim, C.-H., Lin, C.-Y., Chen, L., Zhang, M., Tao, Z., Li, J., Kajino, M., Liao, H., Wang, Z., Sudo, K., Wang, Y., Pan, Y., Tang, G., Li, M., Wu, Q., Ge, B., and Carmichael, G. R.: Evaluation and uncertainty investigation of the NO₂, CO and NH₃ modeling over China under the framework of MICS-Asia III, *Atmos. Chem. Phys.*, 20, 181–202, <https://doi.org/10.5194/acp-20-181-2020>, 2020.
- Kuribayashi, M., Ohara, T., Morino, Y., Uno, I., Kurokawa, J., and Hara, H.: Long-term trends of sulfur deposition in East Asia, *Atmos. Environ.*, 59, 461–475, <https://doi.org/10.1016/j.atmosenv.2012.04.060>, 2012.
- Kurokawa, J., Ohara, T., Morikawa, T., Hanayama, S., Janssens-Maenhout, G., Fukui, T., Kawashima, K., and Akimoto, H.: Emissions of air pollutants and greenhouse gases over Asian regions during 2000–2008: Regional Emission inventory in ASia (REAS) version 2, *Atmos. Chem. Phys.*, 13, 11019–11058, <https://doi.org/10.5194/acp-13-11019-2013>, 2013.
- Lee, D. G., Lee, Y.-M., Jang, K.-W., Yoo, C., Kang, K.-H., Lee, J.-H., Jung, S.-W., Park, J.-M., Lee, S.-B., Han, J.-S., Hong, J.-H., and Lee, S.-J.: Korean national emissions inventory system and 2007 air pollutant emissions, *Asian J. Atmos. Environ.*, 5, 278–291, 2011.
- Li, J., Wang, Z., Wang, X., Yamaji, K., Takigawa, M., Kanaya, Y., Pochanart, P., Liu, Y., Irie, H., Hu B., Tanimoto, H., and Akimoto, H.: Impacts of aerosols on summertime tropospheric photolysis frequencies and photochemistry over Central Eastern China, *Atmos. Environ.*, 45, 1817–1829, 2011.
- Li, J., Yang, W., Wang, Z., Chen, H., Hu, B., Li, J., Sun, Y., Fu, P., and Zhang, Y.: Modeling study of surface ozone source-receptor relationships in East Asia, *Atmos. Res.*, 167, 77–88, 2016.
- Li, J., Nagashima, T., Kong, L., Ge, B., Yamaji, K., Fu, J. S., Wang, X., Fan, Q., Itahashi, S., Lee, H.-J., Kim, C.-H., Lin, C.-Y., Zhang, M., Tao, Z., Kajino, M., Liao, H., Li, M., Woo, J.-H., Kurokawa, J., Wang, Z., Wu, Q., Akimoto, H., Carmichael, G. R., and Wang, Z.: Model evaluation and intercomparison of surface-level ozone and relevant species in East Asia in the context of MICS-Asia Phase III – Part 1: Overview, *Atmos. Chem. Phys.*, 19, 12993–13015, <https://doi.org/10.5194/acp-19-12993-2019>, 2019.
- Li, M., Zhang, Q., Kurokawa, J.-I., Woo, J.-H., He, K., Lu, Z., Ohara, T., Song, Y., Streets, D. G., Carmichael, G. R., Cheng, Y., Hong, C., Huo, H., Jiang, X., Kang, S., Liu, F., Su, H., and Zheng, B.: MIX: a mosaic Asian anthropogenic emission inventory under the international collaboration framework of the MICS-Asia and HTAP, *Atmos. Chem. Phys.*, 17, 935–963, <https://doi.org/10.5194/acp-17-935-2017>, 2017a.
- Li, M., Liu, H., Geng, G., Hong, C., Liu, F., Song, Y., Tong, D., Zheng, B., Cui, H., Man, H., Zhang, Q., and He, K.: Anthropogenic emission inventories in China: a review, *Nat. Sci. Rev.*, 4, 834–866, 2017b.
- Lin, M., Oki, T., Bengtsson, M., Kanae, S., Halloway, T., and Streets, D. G.: Long-range transport of acidifying substances in East Asia—Part II: Source-receptor relationships, *Atmos. Environ.*, 42, 5956–5967, <https://doi.org/10.1016/j.atmosenv.2008.03.039>, 2008.
- Liu, H., Jacob, D. J., Bey, I., and Yantosca, R. M.: Constraints from ²¹⁰Pb and ⁷Be on wet deposition and transport in a global three-dimensional chemical, *J. Geophys. Res.*, 2001, 106, 12109–12128, 2001.
- Lu, Z. and Streets, D. G.: Increase in NO_x emissions from Indian thermal power plants during 1996–2010: Unit-based inventories and multisatellite observations, *Environ. Sci. Technol.*, 46, 7463–7470, <https://doi.org/10.1021/es300831w>, 2012.
- Lu, Z., Zhang, Q., and Streets, D. G.: Sulfur dioxide and primary carbonaceous aerosol emissions in China and India, 1996–2010, *Atmos. Chem. Phys.*, 11, 9839–9864, <https://doi.org/10.5194/acp-11-9839-2011>, 2011.
- Matsui, T., Zhang, S. Q., Tao, W.-K., Lang, S., Ichoku, C., and Peters-Lidard, C.: Impact of radiation frequency, precipitation radiative forcing, and radiation column aggregation on convection-permitting West African Monsoon simulations, *Clim. Dynam.*, 1–21, <https://doi.org/10.1007/s00382-018-4187-2>, 2018.
- Mlawer, E. J., Taubman, S. J., Brown, P. D., Iacono, M. J., and Clough, S. A.: Radiative transfer for inhomogeneous atmospheres: RRTM, a validated correlated-k model for the long-wave, *J. Geophys. Res.*, 102, 16663–16682, 1997.
- Morino, Y., Ohara, T., Kurokawa, J., Kuribayashi, M., Uno, I., and Hara, H.: Temporal variations of nitrogen wet deposition across Japan from 1989 to 2008, *J. Geophys. Res.-Atmos.*, 116, D06307, <https://doi.org/10.1029/2010JD015205>, 2011.
- NASA: Global Modeling and Assimilation Office (GMAO), available at: <https://gmao.gsfc.nasa.gov>, last access: 14 February 2020.
- NCEP/NCAR: Final Analysis Data (FNL), available at: <http://rda.ucar.edu/datasets/ds083.2/>, last access: 14 February 2020.
- Nenes, A., Pandis, S. N., and Pilinis, C.: ISORROPIA: A new thermodynamic equilibrium model for multiphase multicomponent inorganic aerosols, *Aquat. Geochem.*, 4, 123–152, 1998.
- Park, R. J., Jacob, D. J., Field, B. D., and Yantosca, R. M.: Natural and transboundary pollution influences on sulfate-nitrate-ammonium aerosols in the United States: Implications for policy, *J. Geophys. Res.*, 109, D15204, <https://doi.org/10.1029/2003jd004473>, 2004.
- Pielke, R. A., Cotton, W. R., Walko, R. L., Trenback, C. J., Lynos, W. A., Grasso, L. D., Nicholls, M. E., Moran, M. D., Wesley, D. A., Lee, T. J., and Copeland, J. H.: A comprehensive meteorological modeling system-RAMS, *Meteorol. Atmos. Phys.*, 49, 69–91, 1992.
- Pleim, J. E.: A combined local and nonlocal closure model for the atmospheric boundary layer, Part I: Model description and testing, *J. Appl. Meteorol. Clim.*, 46, 1383–1395, 2007a.

- Pleim, J. E.: A combined local and nonlocal closure model for the atmospheric boundary layer. Part II: Application and evaluation in a mesoscale meteorological model, *J. Appl. Meteorol. Clim.*, 46, 1396–1409, 2007b.
- Pleim, J. E. and Chang, J. S.: A non-local closure model for vertical mixing in the convective boundary layer, *Atmos. Environ. A-Gen.*, 26, 965–981, [https://doi.org/10.1016/0960-1686\(92\)90028-J](https://doi.org/10.1016/0960-1686(92)90028-J), 1992.
- Pleim, J. E., Xiu, A., Finkelstein, P. L., and Otte, T. L.: A coupled land-surface and dry deposition model and comparison to field measurements of surface heat, moisture, and ozone fluxes, *Water Air Soil Pollut. Focus*, 1, 243–252, <https://doi.org/10.1023/A:1013123725860>, 2001.
- Pye, H. O. T., Liao, H., Wu, S., Mickley, L. J., Jacob, D. J., Henze, D. K., and Seinfeld, J. H.: Effect of changes in climate and emissions on future sulfate-nitrate-ammonium aerosol levels in the United States, *J. Geophys. Res.*, 114, D01205, <https://doi.org/10.1029/2008jd010701>, 2009.
- Shao, J., Chen, Q., Wang, Y., Lu, X., He, P., Sun, Y., Shah, V., Martin, R. V., Philip, S., Song, S., Zhao, Y., Xie, Z., Zhang, L., and Alexander, B.: Heterogeneous sulfate aerosol formation mechanisms during wintertime Chinese haze events: air quality model assessment using observations of sulfate oxygen isotopes in Beijing, *Atmos. Chem. Phys.*, 19, 6107–6123, <https://doi.org/10.5194/acp-19-6107-2019>, 2019.
- Simon, H. and Bhade, P. V.: Simulating the degree of oxidation in atmospheric organic particles, *Environ. Sci. Technol.*, 46, 331–339, <https://doi.org/10.1021/es202361w>, 2012.
- Skamarock, W. C., Klemp, J. B., Dudhia, J., Gill, D. D., Barker, D. M., Duda, M. G., Huang, X.-Y., Wang, W., and Powers, J. G.: A description of the advanced research WRF version 3, *Nat. Cent. Atmos. Res.*, Boulder, CO, NCAR Technical Note, NCAR/TN-475+STR, 113 pp., 2008.
- Solazzo, E., Bianconi, R., Pirovano, G., Matthias, V., Vautard, R., Appel, K. W., Bessagnet, B., Brandt, J., Christensen, J. H., Chemel, C., Coll, I., Ferreira, J., Forkel, R., Francis, X. V., Grell, G., Grossi, P., Hansen, A., Miranda, A. I., Moran, M. D., Nopmongco, U., Parnk, M., Sartelet, K. N., Schaap, M., D. Silver, J., Sokhi, R. S., Vira, J., Werhahn, J., Wolke, R., Yarwood, G., Zhang, J., Rao, S. T., and Galmarin, S.: Model evaluation and ensemble modelling of surface-level ozone in Europe and North America in the context of AQMEII, *Atmos. Environ.*, 53, 60–74, 2012.
- Sudo, K., Takahashi, M., Kurokawa, J. I., and Akimoto, H.: CHASER: A global chemical model of the troposphere 1. Model description, *J. Geophys. Res.*, 107, 4339, <https://doi.org/10.1029/2001JD001113>, 2002a.
- Sudo, K., Takahashi, M., and Akimoto, H.: CHASER: A global chemical model of the troposphere 2. Model results and evaluation, *J. Geophys. Res.*, 107, 4586, <https://doi.org/10.1029/2001JD001114>, 2002b.
- Tan, J., Fu, J. S., Carmichael, G. R., Itahashi, S., Tao, Z., Huang, K., Dong, X., Yamaji, K., Nagashima, T., Wang, X., Liu, Y., Lee, H.-J., Lin, C.-Y., Ge, B., Kajino, M., Zhu, J., Zhang, M., Hong, L., and Wang, Z.: Why models perform differently on particulate matter over East Asia? – A multi-model intercomparison study for MICS-Asia III, *Atmos. Chem. Phys. Discuss.*, <https://doi.org/10.5194/acp-2019-392>, in review, 2019.
- Tewari, M., Chen, F., Wang, W., Dudhia, J., LeMone, M. A., Mitchell, K., Ek, M., Gayno, G., Wegiel, J., and Cuenca, R. H.: Implementation and verification of the unified NOAH land surface model in the WRF model, 20th conference on weather analysis and forecasting/16th conference on numerical weather prediction, 11–15, 2004.
- van der Werf, G. R., Randerson, J. T., Giglio, L., Collatz, G. J., Mu, M., Kasibhatla, P. S., Morton, D. C., DeFries, R. S., Jin, Y., and van Leeuwen, T. T.: Global fire emissions and the contribution of deforestation, savanna, forest, agricultural, and peat fires (1997–2009), *Atmos. Chem. Phys.*, 10, 11707–11735, <https://doi.org/10.5194/acp-10-11707-2010>, 2010.
- Vet, R., Artz, R. S., Carou, S., Shaw, M., Ro, C. -U., Aas, W., Baker, A., Bowersox, V. C., Dentener, F., Galy-Lacaux, C., Hou, A., Piennar, J. J., Gillett, R., Forti, M. C., Gromov, S., Hara, H., Khodzher, T., Mahowald, N. M., Nickovic, S., Rao, P. S. P., and Reid, N. W.: A global assessment of precipitation chemistry and deposition of sulfur, nitrogen, sea salt, base cations, organic acids, acidity and pH, and phosphorous, *Atmos. Environ.*, 93, 3–100, <https://doi.org/10.1016/j.atmosenv.2013.10.060>, 2014.
- Walcek, C. J. and Aleksic, N. M.: A simple but accurate mass conservative peak-preserving, mixing ratio bounded advection algorithm with fortran code, *Atmos. Environ.*, 32, 3863–3880, 1998.
- Wang, Y. X., McElroy, M. B., Jacob, D. J., and Yantosca, R. M.: A nested grid formulation for chemical transport model over Asia: Applications to CO, *J. Geophys. Res.*, 109, D22307, <https://doi.org/10.1029/2004JD005237>, 2004.
- Wang, Z., Maeda, T., Hayashi, M., Hsiao, L. F., and Liu, K. Y.: A nested air quality prediction modeling system for urban and regional scales: application for high ozone episode in Taiwan, *Water Air Soil Pollut.*, 130, 391–396, 2001.
- Wang, Z., Xie, F., Sakurai, T., Ueda, H., Han, Z., Carmichael, G. R., Streets, D., Engards, M., Holloway, T., Hayami, H., Kajino, M., Thongboonchoo, N., Bennet, C., Park, S. U., Fung, C., Chang, A., Sartelet, K., and Amann, M.: MICS-Asia II: Model intercomparison and evaluation of acid deposition, *Atmos. Environ.*, 42, 3528–3542, <https://doi.org/10.1016/j.atmosenv.2007.12.071>, 2008.
- Wesely, M. L.: Parameterization of surface resistance to gaseous dry deposition in regional numerical models, *Atmos. Environ.*, 16, 1293–1304, 1989.
- Wesely, M. L. and Hicks, B. B.: Some factors that affect the deposition rates of sulfur dioxide and similar gases on vegetation, *J. Air Pollut. Control Assoc.*, 27, 1110–1116, 1977.
- World Meteorological Organization Global Atmosphere Watch: Global Atmosphere Watch Workshop on Measurement-Model Fusion for Global Total Atmospheric Deposition (MMF-GTAD), World Meteorological Organization, Geneva, Switzerland, GAW Report No. 234, 2017.
- Xu, W., Luo, X. S., Pan, Y. P., Zhang, L., Tang, A. H., Shen, J. L., Zhang, Y., Li, K. H., Wu, Q. H., Yang, D. W., Zhang, Y. Y., Xue, J., Li, W. Q., Li, Q. Q., Tang, L., Lu, S. H., Liang, T., Tong, Y. A., Liu, P., Zhang, Q., Xiong, Z. Q., Shi, X. J., Wu, L. H., Shi, W. Q., Tian, K., Zhong, X. H., Shi, K., Tang, Q. Y., Zhang, L. J., Huang, J. L., He, C. E., Kuang, F. H., Zhu, B., Liu, H., Jin, X., Xin, Y. J., Shi, X. K., Du, E. Z., Dore, A. J., Tang, S., Collett Jr., J. L., Goulding, K., Sun, Y. X., Ren, J., Zhang, F. S., and Liu, X. J.: Quantifying atmospheric nitrogen deposition through a nationwide monitoring network across China, *Atmos. Chem.*

- Phys., 15, 12345–12360, <https://doi.org/10.5194/acp-15-12345-2015>, 2015.
- Yamartino, R. J.: Nonnegative, conserved scalar transport using grid-cell-centered, spectrally constrained Blackman cubics for applications on a variable-thickness mesh, *Mon. Weather Rev.*, 121, 753–763, 1993.
- Zaveri, R. A. and Peters, L. K.: A new lumped structure photochemical mechanism for large-scale applications, *J. Geophys. Res.*, 104, 30387–30415, 1999.
- Zhang, Y., Mathur, R., Bash, J. O., Hogrefe, C., Xing, J., and Roselle, S. J.: Long-term trends in total inorganic nitrogen and sulfur deposition in the US from 1990 to 2010, *Atmos. Chem. Phys.*, 18, 9091–9106, <https://doi.org/10.5194/acp-18-9091-2018>, 2018.
- Zheng, B., Zhang, Q., Zhang, Y., He, K. B., Wang, K., Zheng, G. J., Duan, F. K., Ma, Y. L., and Kimoto, T.: Heterogeneous chemistry: a mechanism missing in current models to explain secondary inorganic aerosol formation during the January 2013 haze episode in North China, *Atmos. Chem. Phys.*, 15, 2031–2049, <https://doi.org/10.5194/acp-15-2031-2015>, 2015.